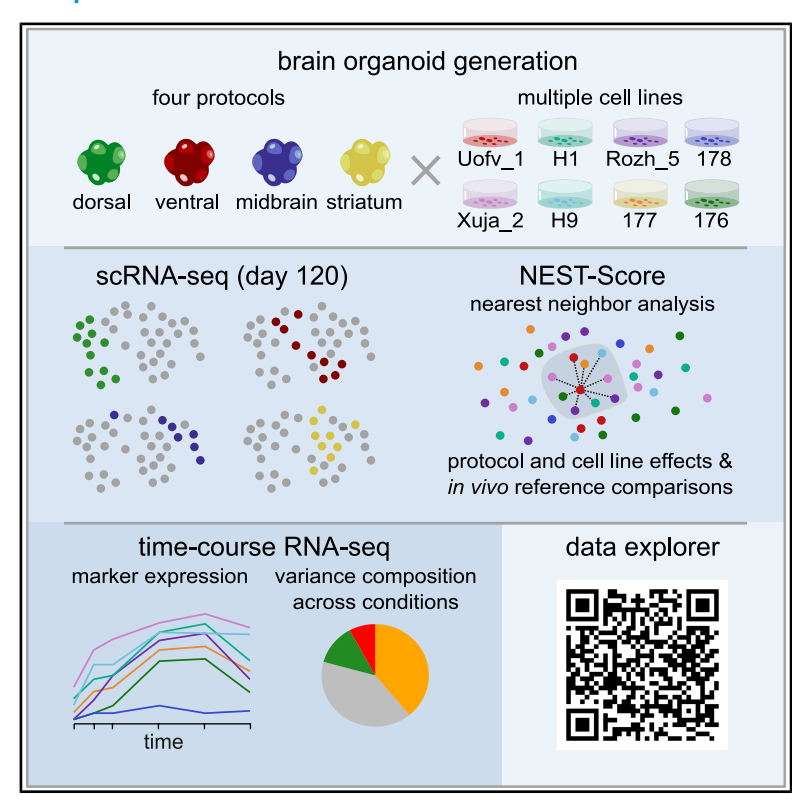
## Quantitative profiling of human brain organoid cell diversity across four protocols and multiple cell lines

### **Graphical abstract**



### **Authors**

Julia Naas, Meritxell Balmaña, Laurenz Holcik, ..., Arndt von Haeseler, Christopher Esk, Jürgen A. Knoblich

### Correspondence

arndt.von.haeseler@univie.ac.at (A.v.H.), christopher.esk@uibk.ac.at (C.E.), juergen.knoblich@imba.oeaw.ac.at (J.A. K.)

### In brief

Naas et al. analyzed brain organoids from multiple cell lines in four regional protocols using scRNA-seq and timeresolved RNA-seq. They apply a computational tool, the "NEST-Score", to identify cell-line- and protocol-driven cells in organoids and compare to *in vivo* references. Analyses and visualizations are provided via a web explorer.

### **Highlights**

- Four brain organoid protocols from multiple cell lines recapitulating in vivo cells
- scRNA-seq of all conditions at day 120 and time-resolved RNA-seq
- NEST-Score for comparisons of multiplexed scRNA-seq data
- Resource for data exploration: https:// vienna-brain-organoid-explorer.vbc.ac.at







### Resource

# Quantitative profiling of human brain organoid cell diversity across four protocols and multiple cell lines

Julia Naas, 1,2,10 Meritxell Balmaña, 3,10 Laurenz Holcik, 1,2 Maria Novatchkova, Lina Dobnikar, Thomas Krausgruber, 4,5 Sabrina Ladstätter, Christoph Bock, 4,5 Arndt von Haeseler, 1,6,7,\* Christopher Esk, 3,8,\* and Jürgen A. Knoblich 3,9,11,\* Center for Integrative Bioinformatics Vienna (CIBIV), Max Perutz Labs, University of Vienna and Medical University of Vienna, Vienna BioCenter, Vienna, Austria

### **SUMMARY**

Human brain organoids are powerful *in vitro* models for brain development and disease. However, protocol and pluripotent cell line choices influence organoid variability and cell-type representation, complicating their use in biomedical research. Here, we systematically analyze the cellular and transcriptional landscape of brain organoids across multiple cell lines using four protocols aimed at recapitulating dorsal and ventral forebrain, midbrain, and striatum. We introduce the *NEST-Score* to evaluate cell-line- and protocol-driven differentiation propensities and comparisons to *in vivo* references. Thereby, we establish a set of protocols that together recreate the majority of cell types in the developing brain and provide a reference of cell-type recapitulation across cell lines and protocols. Additionally, we identify early gene expression signatures predicting protocol-driven organoid generation. We provide easy access to our data through a web explorer, creating a reference for brain organoid research and allowing straightforward protocol and cell-line performance validation.

### **INTRODUCTION**

Human brain organoids are three-dimensional, self-organizing in vitro models that recapitulate functional as well as structural aspects of the developing brain. 1-13 In order to capture the neuronal complexity of the brain, a variety of protocols have been established to model the development of specific brain regions, such as dorsal or ventral forebrain or midbrain. 14-19 Publications describing organoid protocols typically include evidence showing that the right cell types are generated; but variability across samples and cell lines has been a challenge. 8,20-22 Cell lines can have intrinsic biases so that individual cell types are created in variable amounts. Furthermore, a strong cell line bias can lead to the formation of cell types that are not present in the tissue to be modeled. Without additional information, it is impossible to determine whether a transcriptomic state of an organoid's cell is driven by cell line intrinsic properties or guidance cues of a protocol. This poses a challenge to any study using patient-derived cell lines as it is unclear whether phenotypic effects

are consequences of the genetic background, disease-associated genetic variants, or due to other cell-line- or protocol-driven variability.

To define reference protocol signatures that are independent of the specific cell line used, we systematically evaluated four organoid growth protocols based on two success factors: (1) the reliable generation of the same cell types across multiple cell lines and (2) the generation of cell types that form the respective target brain region in vivo. Toward this goal, we provide a comprehensive dataset that evaluates (1) intrinsic biases of cell lines within a given brain organoid protocol, (2) reliability of protocols across multiple cell lines, and (3) similarity between the cells generated in vitro and in vivo. We examined four protocols guiding organoid growth toward dorsal forebrain, ventral forebrain, midbrain, and striatum by conducting single-cell RNA sequencing (scRNA-seg) experiments on mature organoids and time-resolved bulk RNA-seq. For each protocol, we distinguish protocol-driven cell states formed across multiple cell lines from cell line-driven cell states only observed in



<sup>&</sup>lt;sup>2</sup>Vienna Biocenter PhD Program, a Doctoral School of the University of Vienna and Medical University of Vienna, Vienna, Austria

<sup>&</sup>lt;sup>3</sup>Institute of Molecular Biotechnology of the Austrian Academy of Science (IMBA), Vienna BioCenter (VBC), Vienna, Austria

<sup>&</sup>lt;sup>4</sup>CeMM Research Center for Molecular Medicine of the Austrian Academy of Sciences, Vienna, Austria

<sup>&</sup>lt;sup>5</sup>Medical University of Vienna, Institute of Artificial Intelligence, Center for Medical Data Science, Vienna, Austria

<sup>&</sup>lt;sup>6</sup>Bioinformatics and Computational Biology, Faculty of Computer Science, University of Vienna, Vienna, Austria

<sup>&</sup>lt;sup>7</sup>Ludwig Boltzmann Institute for Network Medicine at the University of Vienna, Vienna, Austria

<sup>&</sup>lt;sup>8</sup>Institute of Molecular Biology, University of Innsbruck, Innsbruck, Austria

<sup>&</sup>lt;sup>9</sup>Medical University of Vienna, Vienna BioCenter (VBC), Vienna, Austria

<sup>&</sup>lt;sup>10</sup>These authors contributed equally

<sup>&</sup>lt;sup>11</sup>Lead contact

<sup>\*</sup>Correspondence: arndt.von.haeseler@univie.ac.at (A.v.H.), christopher.esk@uibk.ac.at (C.E.), juergen.knoblich@imba.oeaw.ac.at (J.A.K.) https://doi.org/10.1016/j.celrep.2025.116168



few cell lines. Thereby, we determine the reliable generation of cell types, the first success factor of a protocol. In addition, we measure how well brain organoid cell types match in vivo counterparts as the second success factor. To quantify both success factors, we have developed the NEST-Score (neighborhood sample homogeneity-score) that evaluates how well different samples cover the transcriptomic state of each cell based on its neighborhood in principle component space. In each protocol, we demonstrate that more than half of the considered cell lines contribute predominantly to protocoldriven cell states, the majority of which recapitulates cells found in vivo. 23,24 To understand whether the success of a protocol can already be assessed at early stages, we performed time-resolved bulk RNA-seq across all protocols and seven cell lines. This allows us to obtain cell-line-independent, protocol-specific marker gene sets that may serve as reference for future brain organoid experiments. We provide easy open access to our data via a web-based data explorer, which enables simultaneous browsing across both scRNA and bulk RNA-seq data for individual genes or gene groups of interest (https:// vienna-brain-organoid-explorer.vbc.ac.at).

### **RESULTS**

## Brain organoid single-cell RNA-seq across protocols and cell lines

To explore a large variety of cell types generated in vitro, we employed four distinct brain organoid protocols designed to generate dorsal and ventral forebrain, midbrain, and striatum tissue using eight different cell lines for organoid generation. We examined the cellular composition of 120-day-old organoids in duplicates using droplet-based scRNA-seq (10X Genomics) (Figures 1A and S1A). Organoids were grown to day 120 because at that time point, most major mature neuronal cell types are created while a diverse population of progenitor cells is retained. 8,25-27 All conditions were grown and sequenced in parallel to minimize batch variability, eliminating the need for subsequent computational batch correction. Quality control filtering<sup>28</sup> retained approximately 70,000 high-quality single-cell transcriptomes for downstream analysis (see STAR Methods) (Figures 1B and S1A). High-quality cells in the combined dataset encompassing all protocols and cell lines reveal cell clusters that were annotated based on marker gene expression and previous literature<sup>8,22,25,27</sup> and visualized using uniform manifold approximation and projection (UMAP). We identified a wide range of glial and neuronal cell types in distinct clusters that reflect neuron maturation (Figure 1B; Tables S1 and S2). The differentiation of glial cells to neurons from different dorsal, ventral, midbrain, and striatal brain regions can be traced as individual trajectories in the combined UMAP. For instance, the well-documented differentiation of excitatory neurons from dorsal radial glia (marked by PAX6 and HOPX expression) through intermediate progenitors (EOMES expression) into immature, deep, and upper layer neurons (SLA, TBR1, and SATB2 expression, respectively) forms a distinct set of clusters. This trajectory is separate from ventral, inhibitory progenitors and neurons (DLX2, SST expression) as well as floorplate progenitors (FOXA2 expression) and midbrain-like cells (EN1 expression). We observed that midbrain and ventral inhibitory forebrain

progenitors clustered relatively close together, suggesting a more gradual difference between their gene expression profiles compared to dorsal progenitors (Figure 1B). Additionally, cells of hindbrain identity or photoreceptor cells and cells of non-neural origin such as muscle (DES expression) and stromal cells (COL3A1 expression) can be observed (Figure S1B).

In the combined dataset, cells derived from dorsal, ventral, and midbrain protocols occupy different transcriptional states (Figures 1C and S1C). Cells of the excitatory neuronal lineage originated from organoids grown in the dorsal protocol, while the ventral protocol predominantly contributed to the development of inhibitory neurons. The midbrain protocol generated midbrain progenitor clusters and contributed to midbrain-like cells (Figures 1B, 1C, and S1C). In contrast, the striatum protocol produced cell states that were also found in the other three protocols, but additionally generated unique cells not produced by the other three protocols. These striatum-protocol-specific cells express markers consistent with medium spiny neuron identity (SIX3, SP9 expression) (Figure S1B). Overall, the four differentiation protocols across all cell lines collectively yield a highly diverse array of cell types, underscoring the potential of brain organoid protocols to model many neural cell types of the developing human brain (Figure 1D).

To link cells produced in the four protocols to their corresponding anatomical locations, we correlated our data with spatially resolved transcriptome data from comparable mouse brain slices (Allen Developing Mouse Brain Atlas<sup>30,31</sup>). To do so, we used VoxHunt,<sup>29</sup> an algorithm that was previously introduced and validated to assess regional identity of human brain organoids in comparison to spatial transcriptomic mouse data (Figure 1E). Cells from each protocol generally matched well to the corresponding anatomical mouse brain region, indicating that the organoids are patterned as expected. However, upon closer inspection, minor positive correlation of gene expression profiles was also observed with unexpected brain regions, such as cells from the midbrain protocol correlating with mouse ventral forebrain structures. Indeed, cell-type clusters annotated to be midbrain progenitors or midbrain-like correlated better with the corresponding midbrain reference than the sum of midbrain protocol-derived cells, indicating that protocols contained additional non-targeted cells (compare Figures 1E and S1D). This observation led us to split the combined UMAP by both individual cell line and protocol (Figure S1E) revealing that individual cell lines vary in the degree to which they contribute to cell types generated within each protocol. While most cell lines generated cells consistent with cell types targeted by the respective protocols, some produced aberrant cell types. In the midbrain protocol, for example, cell line Uofv\_1 produced a considerable number of inhibitory neurons that align with those generated in the ventral forebrain protocol (Figure S1C). In the dorsal protocol, cell lines 176 and Xuja\_2 gave rise to different non-neural tissues (muscle and stromal cells). As such unintended cell types were generated only from few cell lines, they can be recognized by a low degree of intermixing with cells from other cell lines. This indicates that inherent tendencies of certain cell lines can override the guidance cues provided by a protocol, prompting us to categorize these instances by determining whether a cell state is consistently produced within a protocol.

### Resource



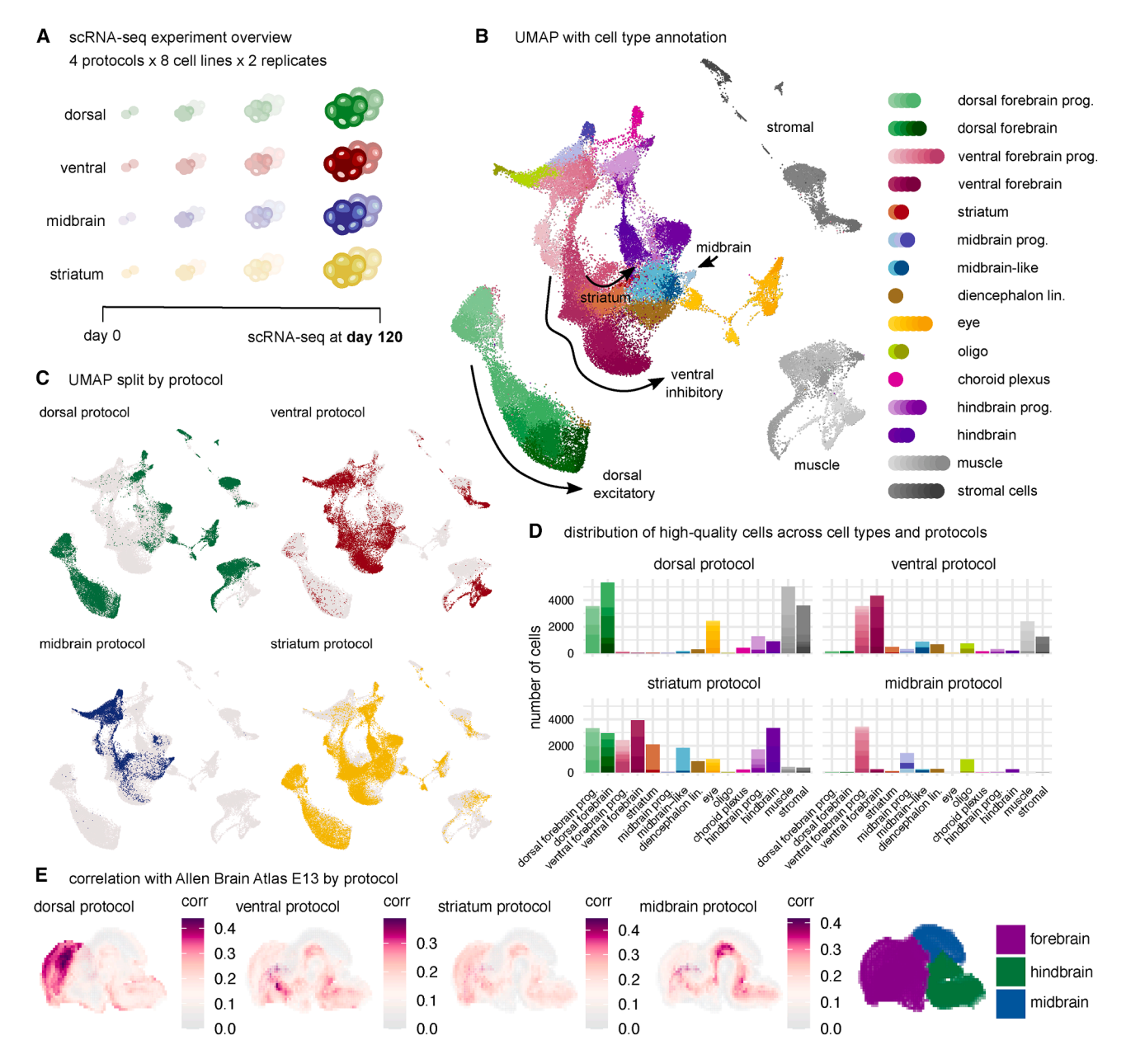


Figure 1. The transcriptional potential of organoids grown from multiple protocols and cell lines at single-cell resolution (also see Figure S1)

- (A) Experimental overview for endpoint scRNA-seq analysis of brain organoids from four protocols and eight cell lines.
- (B) UMAP embedding of scRNA-seq data across four protocols and eight cell lines, color-coded by annotated cell types. prog., progenitors; lin., lineage.
- (C) UMAP of scRNA-seq data colored by the protocol of origin.
- (D) Contribution of protocols to annotated cell types of the scRNA-seq dataset.

(E) VoxHunt<sup>29</sup> analysis of organoid scRNA-seq data with spatial transcriptomics data of a mouse brain slice at embryonic day 13 (Allen Developing Mouse Brain Atlas<sup>30,31</sup>) shows protocol-specific Spearman correlation patterns.

## **Definition of protocol-driven and cell-line-driven cell states**

To assess how reliable specific cell types are generated in one protocol from multiple cell lines, we devised the *NEST-Score* (Figure 2A; STAR Methods). Computed for each individual cell, this score measures the degree to which a cell's neighborhood is composed of cells from different cell lines. A cell's

maximum score of "0" indicates that this cell's neighborhood is consisting perfectly of all cell lines in the experiment, while a cell's low (negative) NEST-Score indicates that neighboring cells are derived predominantly from the same cell line. Therefore, high NEST-Scores indicate that cells are consistently produced within a given protocol as multiple cell lines generate similar cell states. Vice versa, a cell's low NEST-Score indicates



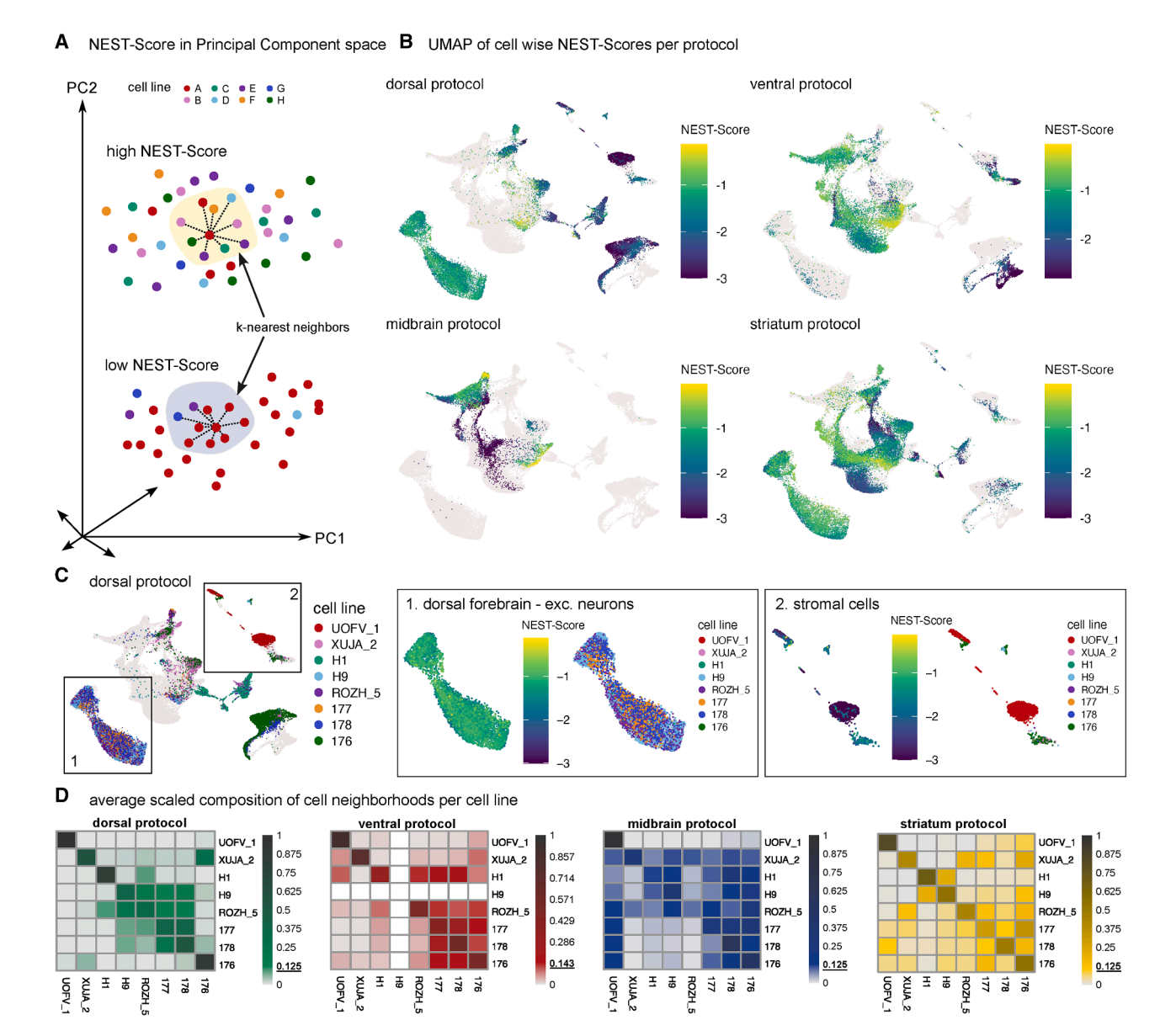


Figure 2. Definition of protocol-driven transcriptional signatures and cell line biases using NEST-scores (also see Figure S2)

(A) Schematic representation of the NEST-Score. High NEST-Scores (close to "0") per cell are the result of neighboring cells originating from many different cell lines (top panel), while low (negative) NEST-Scores indicate that the cell's neighborhood is predominantly composed of cells from the same cell line.

(B) NEST-Score distribution within one protocol depicts protocol-driven cell groups that were consistently developed across multiple cell lines.

(C) Zoom-in dorsal protocol-driven excitatory differentiation lineage (1) and cell-line-driven muscle cells (2) in the dorsal protocol.

(D) Scaled cell line frequencies (STAR Methods) averaged across cells of a given cell line show that cell lines mix well with others within each specific protocol. In a perfect mix cell lines would contribute to  $^{1}$ /<sub>8</sub>= 0.125 of a cell's scaled neighborhood for eight cell lines (dorsal, midbrain, and striatum protocol) and  $1/7 \approx 0.143$  for the seven cell lines in the ventral protocol.

a cell line-driven, non-protocol-conform cell state mainly generated from a particular cell line. Of note, this assessment is independent of how well a cell corresponds to the targeted *in vivo* counterpart (see below for *in vivo* comparisons).

In more detail, for each protocol, we performed principal-component analysis (PCA) on all cells originating from that protocol. Then, for each cell, we determined the cell line origins of its 100 nearest neighbor cells (Figure S2A) by considering the

top principal components. This resulted in a cell-wise cell line frequency vector that was compared to the global cell line frequency vector utilizing the negative Kullback-Leibler divergence<sup>32</sup> (STAR Methods). The NEST-Score reaches its upper bound, "0", when both frequency vectors agree, and hence the respective cell has a neighborhood consisting of all considered cell lines (Figure 2A). By applying a threshold (design dependent on number of cell lines) to the NEST-Scores, we

### Resource



classify each cell in downstream analyses as either protocoldriven (high NEST-Score) or cell-line-driven (low NEST-Score).

Plotting the NEST-Scores of each cell onto the protocol-resolved UMAPs (Figures 2B and 2C) allowed us to visualize how reliably cell lines generate protocol-driven cell types within each protocol. For example, the entire trajectory of dorsal fore-brain progenitors, intermediate progenitors, and excitatory neurons consists of cells with high NEST-Scores, indicating these cell types are consistently produced across multiple cell lines. Similarly, other clusters are consistently produced across cell lines in other protocols (high NEST-Scores), i.e., interneurons in the ventral protocol. Notably, all protocols also contained some cells with low NEST-Scores (Figure 2C), indicating that, in such instances, cells were predominantly mixed with other cells derived from the same cell line. This suggests that such cells and therefore the corresponding cell line did not adhere to a given protocol's guidance cues.

These effects vary across protocols and cell lines and contradict the assumption that protocol guidance cues affect every cell line uniformly. For example, cell line 176 produced mostly protocol-driven cells in ventral, midbrain, and striatum protocols but not in the dorsal protocol, whereas Uofv\_1 predominantly produced cell-line-driven cell types across all four protocols (Figures S1E, S2B, and S2C). This analysis enabled us to evaluate the performance of all cell lines in all protocols individually and to compare them pairwise to identify cell lines that act similarly (STAR Methods). For example, we observed that the four cell lines, H9, Rozh\_5, 177, and 178, produced similar cell states throughout the dorsal protocol (Figure 2D), indicating that cells derived from these cell lines were commonly guided by protocol cues. In contrast, cell lines such as H1, Uofv 1, Xuja\_2, and 176 predominantly mixed only with themselves, consistent with these lines being cell-line-driven in this particular protocol. Analyzing all cell lines in all protocols, we found that individual cell lines may have cell-line-driven biases for cell generation in different protocols, but most growth conditions support the generation of desired protocol-driven cells across cell lines. 19

The use of the NEST-Score is dependent on which cell lines are considered for analysis. When multiple cell lines exhibit similar cell-line-driven biases, cells - and subsequently cell clusters-may be classified as protocol-driven. Therefore, we asked whether protocol-driven cell states and clusters are also the ones that occur in protocols' target tissue, as annotated by region and cell type (Figure 1B).8,22,25,27 When aggregating the NEST-Scores by annotated cell type, we found that all main glial and neuronal cell type clusters visualized in the pan-protocol, pan-cell line UMAP have high scores for the cell types intended by the respective protocol (Figures 2B and S2C). For example, in the dorsal protocol, dorsal progenitors and excitatory neurons were generated across multiple cell lines. In the ventral protocol, instead, ventral progenitors and inhibitory neurons are protocoldriven, and in the midbrain protocol midbrain progenitors are protocol-driven. In contrast, muscle and stromal cells that are found in the dorsal protocol have low NEST-Scores, indicating they were mostly generated by single cell lines (in the dorsal protocol 79.3% of stromal cells derived from cell line Uofv\_1 and 86.40% of muscle cells from cell line 176) (Figures 2C, S2B,

and S2C). Our analysis also identified cell states that are protocol-driven in one protocol but cell-line-driven in another protocol, underlining the necessity for comparing four different protocols. For example, while most cell lines produced protocol-driven cells in the midbrain protocol, one cell line, Uofv\_1, generated cells classified as interneurons (Figures 2B and S2B). Cells of the interneuron lineage are protocol-driven in the ventral and striatum protocols but not the midbrain protocol.

By defining protocol-driven cell states generated from multiple cell lines across four brain organoid protocols and providing the NEST-Score to assess the reliability of cell generation, we provide a framework for protocol benchmarking. The definition of protocol-driven cells per growth protocol thus comprises the first success factor in the application of a robust brain organoid protocol. Importantly, this method can be used to evaluate the suitability of any cell line for growing brain organoids by computing the NEST-Score based on a cell line's scRNA-seq data in combination with the reference datasets provided here. Additionally, the NEST-Score lends itself to evaluate other highly multiplexed scRNA-seq experiments. For example, we evaluated scRNA-seq data from a recent brain organoid morphogen screen, <sup>19</sup> grouping and classifying morphogen combinations that result in similar cell fate acquisition (Figures S2D and S2E).

## Comparison of brain organoid potential to fetal references

Our data allow to distinguish cell-line-driven cell types from cell types that are protocol-driven and consistently generated in a given protocol. To test how well the protocol-driven cell types in the four protocols cover the diversity of cells found in the human brain, we compared them to two commonly referenced in vivo fetal brain tissue datasets. 23,24 One dataset combines forebrain, midbrain, and hindbrain as well as separate dorsal and ventral preparations<sup>24</sup> and a second dataset contains cortical regions.<sup>23</sup> Since both in vivo dataset comparisons gave similar results (Braun et al.<sup>24</sup> comparison Figures 3A-3F, S3A, and S3B; Bhaduri et al.<sup>23</sup> comparison Figures S3C-S3H), we focused on the dataset including more brain regions. We subset the fetal reference to post-conceptional week (pcw) 14, a time point closely resembling day 120 brain organoids based on the timing of glio- and neurogenesis,33 which additionally matches our data in terms of cell number and regions covered, allowing faithful comparisons.<sup>24</sup> Integrating the in vivo reference with our pan-cell line, pan-protocol dataset using Seurat's CCA algorithm into a combined UMAP<sup>34</sup> revealed a large overlap (Figures 3A and 3B; Table S2). In vitro clusters annotated as dorsal and ventral forebrain as well as midbrain progenitors overlap with corresponding in vivo cortex and midbrain clusters. Similarly, in vitro excitatory neurons and inhibitory neurons from dorsal and ventral forebrain show good overlay with their respective in vivo counterparts, while midbrain-like in vitro cells show comparatively looser resemblance to in vivo counterparts. Remaining residual discrepancies between in vivo and in vitro data are expected and indicate that biological variation is not over-corrected. We applied particular care during the integration as we went on to quantify the overlap between in vivo and in vitro in a systematic manner by applying the NEST-Score workflow to access the contribution of in vivo and



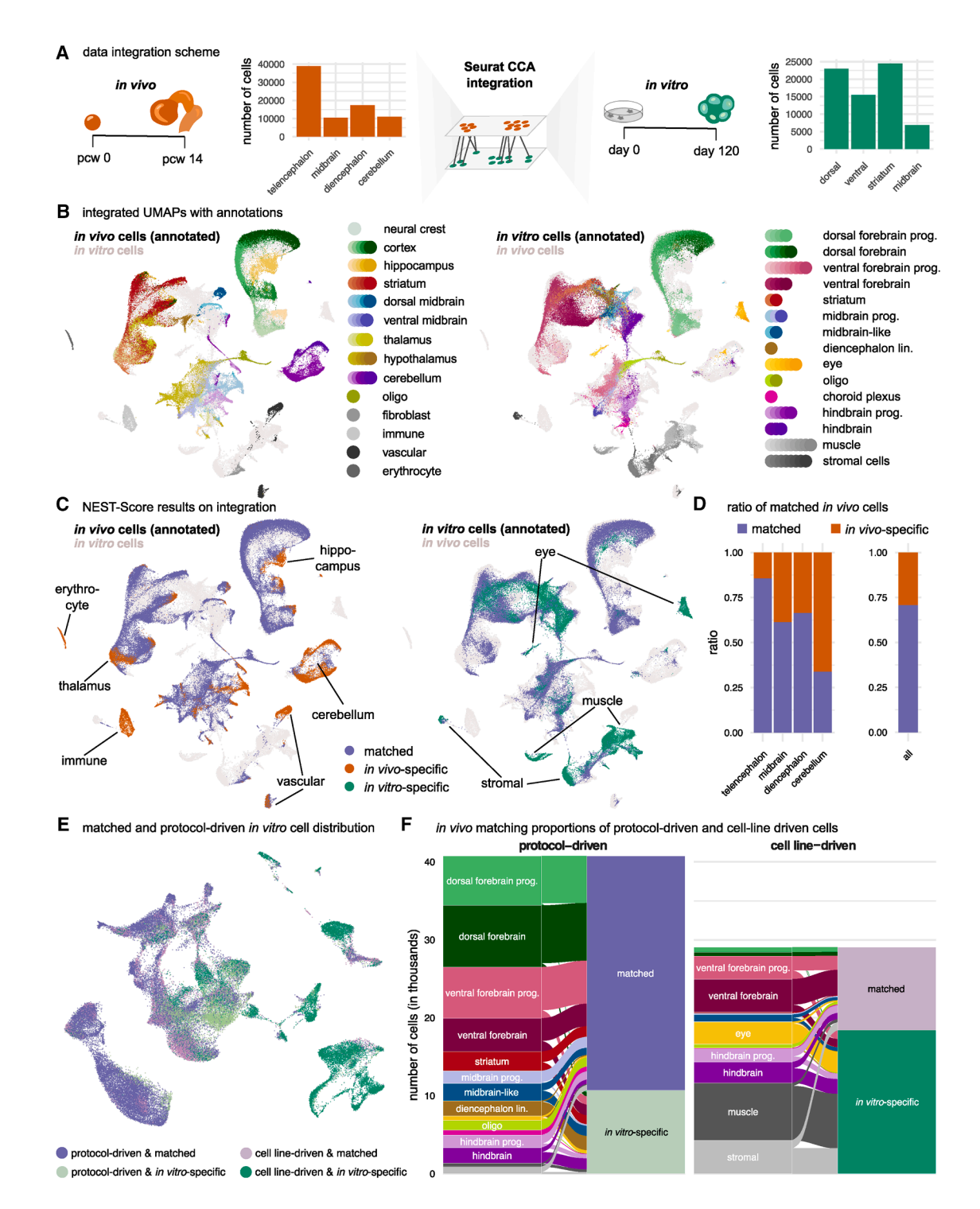


Figure 3. Data integration of in vitro-derived organoid cells with in vivo brain references (also see Figure S3)

(A) Cell numbers of the *in vivo* dataset split by sequenced brain region and cell numbers of the *in vitro* dataset split by protocol. Schematic of Seurat CCA integration of *in vivo* fetal brain samples from post-conceptional week (pcw) 14.<sup>24</sup>

- (B) Sequenced regions of in vivo and annotated, region-specific cell types of in vitro datasets align in the integrated UMAP.
- (C) In vitro/in vivo-matched and -specific cells (STAR Methods) color-coded on the integrated UMAP. Cell types with low in vivo/in vitro overlap are indicated as in vitro-/in vivo-specific.
- (D) Proportions of in vitro-matched and in vivo-specific cells split by in vivo brain regions.
- (E) Integrated in vitro UMAP colored by groups of protocol- or cell-line-driven cells and their overlap with in vivo reference.
- (F) Number of protocol- and cell-line-driven cells split by cell types falling into in vivo-matched and in vitro-specific categories.

### Resource



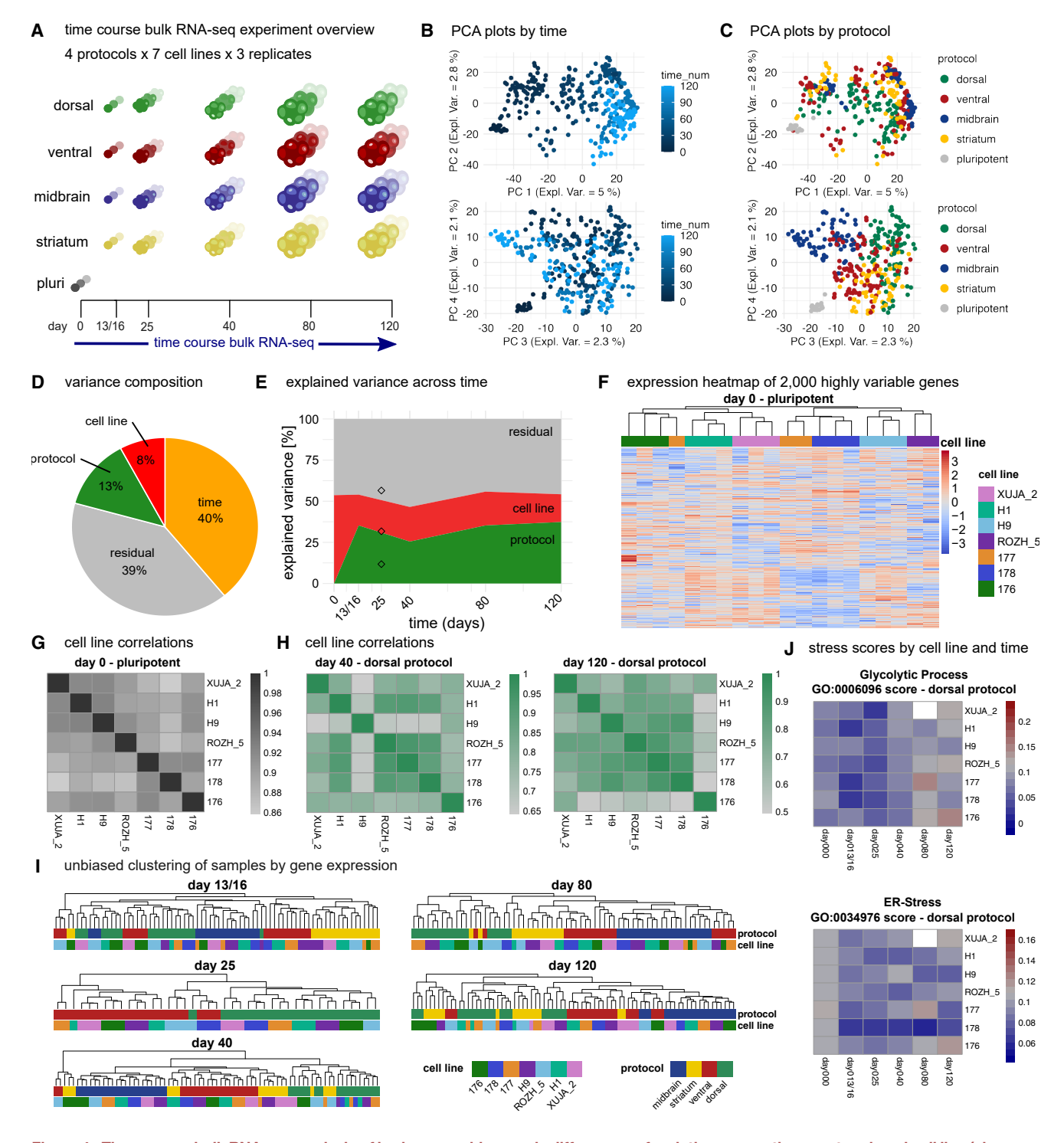


Figure 4. Time course bulk RNA-seq analysis of brain organoids reveals differences of variation across time, protocol, and cell line (also see Figure S4)

- (A) Experimental overview for time course bulk RNA-seq experiment. pluri., pluripotent.
- (B) Principal-component analysis (PCA) of bulk RNA-seq datasets. Plotted are principal components 1 vs. 2 and 3 vs. 4 with samples colored by organoid age.
- (C) PCA of bulk RNA-seq datasets. Plotted are principal components 1 vs. 2 and 3 vs. 4 with samples colored by growth protocol.
- (D) Overall experimental variance split by time, protocol, cell line, and residual.
- (E) Explained variance split by protocol, cell line, and residual across time.
- (F) Hierarchically clustered expression heatmap of 2,000 most highly variable genes on day 0 (pluripotent stem cell stage).

(legend continued on next page)



in vitro samples to a cell's integrated neighborhood (Figures 3C and S3B; STAR Methods). The inspection of NEST-Scores indicated that in vitro and in vivo samples contributed to common cell groups but also that in vitro- and in vivo-specific cell groups existed.

The majority of cell types in the integrated dataset were covered by both in vitro organoid and in vivo fetal cells (Figure 3D). Thereby, in vitro cells in this category fulfill the second success criteria for brain organoid growth in that they resemble in vivo counterparts. Importantly, while each protocol individually allows only limited coverage of the fetal tissue diversity (dorsal protocol covers 41.4%, ventral 50.8%, midbrain 27.3%, and striatum 61.2% of the cells in the in vivo reference dataset) (Figure S3A), combining the four in vitro protocols resulted in an overall representation of 70.6% of all fetal brain cell states (Figure 3D). The remaining 29.4% of the in vivo cells that do not have in vitro cells in their neighborhood include immune cells, erythrocytes, and vascular cells (Figures 3B and 3C), cell types originating outside the brain. We also did not cover all cerebellar cell states, possibly because hindbrain- or cerebellum-specific brain organoid protocols were not included in our study.

We sought to combine our two success factors for organoid growth: (1) generation of protocol-driven cells across cell lines in each protocol and (2) the generation of in vivo matched cell types. In this analysis, we observed that most protocol-driven in vitro cells (namely the major dorsal, ventral, and midbrain progenitor populations) have counterparts in vivo (Figures 3E and 3F). This indicates that successful adherence to protocol cues results predominantly in the production of cell states present in vivo, highlighting the importance of protocol characterization across multiple cell lines to evaluate in vivo cell-type generation. In contrast, most cell-line-driven cells derived from cell lines not adhering to protocol cues do not mix with any in vivo cells from the references. These in vitro cells that originate from 2 or fewer cell lines and at the same time lack explicit in vivo counterparts, include eye, muscle, and stromal cells (Figures 3E, 3F, S2C, and S3B).

### Bulk RNA-seq derived time-resolved transcriptional signatures

Our scRNA-seq analysis was confined to day 120, a time point where a large variety of both progenitor and differentiated cell types can be observed. To test whether organoid development at earlier time points can predict later cell stages, we performed time course bulk RNA-seq experiments to find predictive markers. For all combinations of the four protocols and seven cell lines, we sequenced three replicate organoids at days 13/16, 25, 40, 80, and 120 (Figures 4A and S4A). We also sequenced three samples of each pluripotent stem cell line in the pluripotent state (day 0). PCA analysis of the combined datasets showed a gradient of samples according to organoid age in PC1 and PC2 (Figure 4B), while PC3 and PC4 showed a grouping by protocol (Figure 4C). Interestingly, grouping by

cell line was only visible in PC7 and PC8 (Figure S4B). By quantifying the contribution of each experimental condition to the total variation of the data, 35,36 we found that the sampling time point explains 39.04% of the overall variance, while protocol and cell line choice contribute 13.29% and 8.05%, respectively (Figure 4D). Protocol- and cell-line-induced variability was consistent over time (Figure 4E). In the pluripotent state (day 0), we observed that some cell lines display slightly more similar expression profiles than others (i.e., H1 with Xuja\_2 or 177 with 178; Figure 4F); however, the overall pairwise correlation between all cell lines is very high (Figure 4G), and the cell line grouping is not predictive for common organoid outcomes at later stages (Figures 4H and S4C-S4F). This indicates that gene expression in pluripotent cell lines is insufficient to reliably predict biases in downstream organoid differentiation. Beginning at day 40, we observed a protocol-specific separation of sample-wise expression profiles driven by genes including transcription factors and developmental signaling pathways in line with previous data<sup>37,38</sup> (Figure 4I; Table S3). At that time point we also found that cell lines mainly producing protocol-driven cells largely cluster together (compare Figures S2B and S4C-S4F). However, this prediction does not hold true for all cell lines across all protocols. For example, in the dorsal protocol, cell line similarities differ between day 40 and day 120, showing H9 as an outlier cell line at day 40 and 176 as an outlier cell line at day 120 (Figure 4I). The latter meets the observation of scRNA-seg samples at day 120, where H9 produces abundant protocol-driven cells while 176 does not.

We wanted to understand whether there are communalities between cell lines whose intrinsic biases prevent the production of protocol-driven cells. Given that different cell lines produced different cell-line-driven off-target cells, we asked if there is nonetheless a common feature among cell lines unable to produce protocol-driven cell types at day 120. Many organoid studies describe a connection between increased cellular stress levels and decreased similarity of organoid cells to in vivo data.<sup>22,39,40</sup> Organoid stress may result from growth media conditions and nutrient limitations due to missing vascularization. 41,42 We asked if increased stress less levels might be a correlative with cell-linedriven tissue growth. To this end, we analyzed the bulk RNA-seq samples over time with respect to high expression of genes assigned to Gene Ontology (GO)<sup>43</sup> terms "Glycolytic Process" (GO:0006096) and "response to endoplasmic reticulum stress" (GO:0034976, endoplasmic reticulum [ER]-stress) indicative of a stress response (STAR Methods). ER-stress is readily apparent in the pluripotent stem cell stage at day 0 and decreases after the application of a growth protocol in the first 40 days of organoid growth, consistent with previous data.44 At later time points, both stress scores increase again, but to different extents across cell lines. Indeed, at day 120, in the dorsal protocol high stress scores are observed for cell lines 176 and Xuja\_2, which generated mainly cell line-driven tissue (Figures 4J, S2A, and S4G). This suggests that elevated cellular stress may limit the ability

<sup>(</sup>G) Pearson correlations between cell lines at day 0.

<sup>(</sup>H) Pearson correlations between cell lines at day 40 and 120 in the dorsal protocol.

<sup>(</sup>l) Hierarchically clustered expression grouping based on 2,000 most highly variable genes on days 13/16, 25, 40, 80, and 120.

<sup>(</sup>J) Stress related Gene Ontology gene group expression over time and cell lines.

### Resource



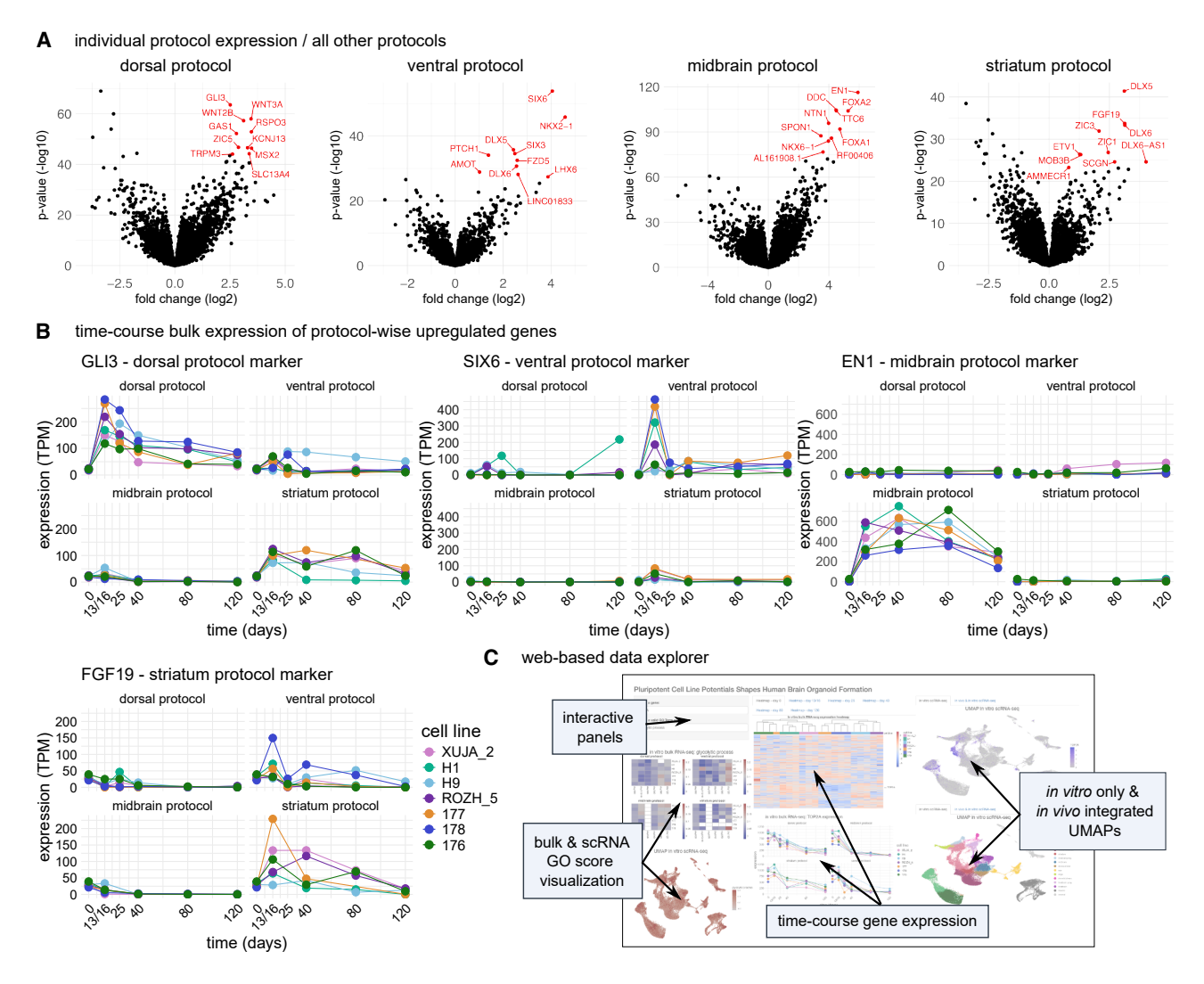


Figure 5. Time course bulk RNA-seq identifies protocol-specific signatures and data explorer overview (also see Figure S5)

(A) Volcano plots of differentially expressed genes tested against all remaining three protocols separated by indicated protocol. Top 10 upregulated genes are indicated.

(B) Gene expression in transcripts per million (TPM) of exemplary protocol markers averaged across all samples of a cell line for each time point. Protocols and marker genes are indicated.

(C) Screenshot of the interactive data browser that allows users to browse through expression profiles of genes of interest in both time course bulk RNA-seq and UMAPs of scRNA-seq data (in vitro only and in vivo integrated) as well as user-defined Gene Ontology analysis.

of cells to respond to protocol cues at late stages of organoid development.

## Protocol-specific markers for successful organoid growth

The time-resolved bulk RNA-seq data allowed us to identify protocol-specific markers independent from individual cell lines. We sought genes that are highly expressed across all cell lines in one protocol compared to all other protocols across all time points (Figure 5A; Table S3). Reassuringly, marker genes identified in this way match expression patterns of protocol-targeted cell types in day 120 scRNA-seq data (Figure S5A). However, this list also includes markers for earlier time points, like SIX6

for the ventral protocol (Figures 5A and 5B), GLI3 for the dorsal protocol, <sup>45</sup> and EN1 and FOXA2 for the midbrain protocol. <sup>46</sup> Besides transcription factors (highlighted in Figure S5B), we also found developmental morphogens (i.e., WNT2B, WNT3A for dorsal protocols) and morphogen receptors (i.e., PTCH1 in the ventral protocol) in line with published data<sup>37</sup> as well as other genes including ion channels (i.e., KCNL13 and TRPM3 in the dorsal protocol) (Figure 5A).

In a second analysis, we concentrated our search for genes that are highly expressed at day 40 in cell lines that produce protocol-driven high-quality organoids at day 120. This results in a marker gene list that is consistent with successful organoid derivation and may serve as a simple quality control readout via



RNA-seq or quantitative real-time PCR of individual organoid batches months before organoids have matured. Day 40 was chosen since this is the earliest time point in which we observe consistent sample separation according to protocol. For each protocol, we tested cell lines yielding a minimum of 75% protocol-driven cells (Figure S2B) against the remaining cell lines in this protocol and all cell lines in the other three protocols at day 40 (Figure S5C; Table S3). The resulting list of upregulated genes again contains expected marker genes (i.e., EOMES, TBR1 in the dorsal protocol, and DLX genes in the ventral protocol) alongside additional putative protocol-specific early regulators of successful organoid derivation.

To make our data easily accessible, we compiled a Shiny App<sup>47</sup> data explorer (https://vienna-brain-organoid-explorer.vbc.ac.at) (Figure 5C). This allows exploration of gene expression signatures for all considered protocols and cell lines across bulk RNA-seq time points and comparisons of *in vivo* and *in vitro* scRNA-seq datasets. Furthermore, it can be used to analyze expression patterns of entire gene sets based on their GO term association, suggesting which biological processes may be important in specific cell types at specific time points and in specific protocols.

### **DISCUSSION**

Brain organoids are widely used in neurodevelopment research and disease modeling, 9,13 but variability across cell lines or protocols makes their use challenging. Here, using four protocols, we provide evidence for generation of large portions (70.6%) of fetal brain cells across several pluripotent stem cell lines. Using multiple cell lines allows to define the propensities of brain organoid protocols for cell modeling, providing a reference for future organoid derivation from additional cell lines. We provide comprehensive scRNA-seq and bulk RNAseq datasets to characterize the four protocols over time and for cell types generated. We introduce the NEST-Score to provide a quantitative measure for reliable generation of cell states across protocols and to evaluate their recapitulation of in vivo cell types. Thereby, we define successful protocols by two factors: the generation of (1) protocol-driven cells across multiple cell lines that (2) match in vivo reference cells. Furthermore, we identify marker gene sets that will allow predictions of organoid protocol success in future work and browsing of all our data using a web portal (https://vienna-brain-organoid-explorer. vbc.ac.at/).

By aligning additional cell lines to our reference and *in vivo* reference data, the NEST-Score can be used to identify protocol-driven cell states for each of the four protocols and to assess how well they match their *in vivo* counterparts. The NEST-Score is particularly useful for the analysis of multiplexed scRNA-seq data that do not require additional batch correction, as we show in the analysis of protocol-driven cells. When evaluating samples with a considerable batch effect, the NEST-Score may also be applied to batch-corrected, integrated data. However, caution should be used in such cases as a reasonable interpretation of the NEST-Score evaluation is only possible, if the strength of the batch effect removal does not remove biological informative variation between samples.

Since the NEST-Score defines cell neighborhoods in PCA space, it is independent from non-linear and oftentimes information-compromising dimensionality reduction methods such as UMAP. It is calculated cell by cell and does not rely on any clustering. Therefore, it is independent of cluster resolutions that might average out cell bias effects. Unlike previous methods, 8,48 it also does not require prior cell-type annotation, making it possible to distinguish the success of a protocol based on (1) reliably producing the same cell states and (2) producing the desired cell types. Our approach shares similarities to other strategies, e.g., the batch effect test kBET<sup>49</sup> or the coverage coefficient.<sup>22</sup> Similarly to the NEST-Score, kBET compares local batch frequencies in a cell's neighborhood with global frequencies but employs the Pearson's  $\mathcal{X}$  test for statistical evaluation. This test is only performed for a subset of cells, and test results (rejection rates) are averaged to access the overall mixing of batches. The test is very sensitive and tends to reject the hypothesis "well mixed" already with one of the batches not contributing to a cell's neighborhood. The NEST-Score is more robust to such outlier data as shown for the application of protocol-driven cells (Figure 2): This comparison included a large amount of different cell lines (=batches), with one cell line Uofv\_1 producing limited protocol-driven cells. In this case, the NEST-Score, which builds on the Kullback-Leibler divergence, enables a more stable and balanced measure to access the mixedness of cell lines. With our scaling scheme of local and global frequencies, the NEST-Score is bounded on both sides and hence provides increased interpretability in contrast to one-side unbounded p values. Other measures, as used in Kanton et al.<sup>20</sup> (reference similarity spectrum [RSS]), Amin et al. 19 (cluster overlap), and He et al. 2 (Max-presence score), are especially developed to compare two datasets, e.g., a query in vitro and a reference in vivo sample, and therefore do not provide a straight-forward analysis of multiple conditions at once.

Our data show that organoid variability is not just a product of protocol stringency and cell line bias. Instead, individual cell lines display distinct biases in a protocol, and a protocol's outcomes should ideally be evaluated from data encompassing a collection of different cell lines, thereby rendering a comprehensive, cell-line-independent protocol characterization.

This work is a step toward the goal of recapitulating all brain cells *in vitro*, with a focus on dorsal and ventral forebrain, midbrain, and striatum. Given that other brain areas, particularly cerebellum, are not included in our current protocol set, we anticipate that brain cell coverage can be further increased in the future by adding protocols addressing, e.g., cerebellum but also non-brain-derived cells including blood vessels and immune cells. Our data complement recent contributions to quantify the transcriptomic diversity of published brain organoid data, citalious a harmonized comparison across different protocols and cell lines without integration/batch-correction simplifying interpretation and quantification of main sources of organoid variability.

Our time course RNA-seq data facilitate the identification of protocol-specific markers that can be tested at early time points in order to predict successful organoid formation, saving time and costs. Our datasets and putative marker lists can also serve as a resource for further optimization of experimental protocols

### Resource



and evaluation of pluripotent cell lines for future research. This may be of particular importance for patient-derived cell lines, which require a solid definition of protocol-driven cells as controls. It also allows us to predict the potential of new cell lines to cover the full spectrum of cell types found *in vivo*.

To facilitate easy access to our data, we implemented a data explorer that visualizes the expression of protocol markers or GO-term-specific gene sets over time, protocol, and cell lines and also in the day 120 scRNA-seq data. The explorer is available at <a href="https://vienna-brain-organoid-explorer.vbc.ac.at">https://vienna-brain-organoid-explorer.vbc.ac.at</a> and allows users to identify marker genes for the formation of specific cell types as well as to choose the right protocol for a specific scientific question.

### **Limitations of the study**

There are several limitations of our study. For example, our current data covers only eight cell lines per protocol. Therefore, future efforts should be geared toward extending the number of cell lines across multiple protocols further. Another limitation is that only four protocols are characterized in-depth. Other studies <sup>19,21</sup> consider larger number of growth conditions but use fewer cell lines and earlier analysis time points, and it will be interesting to cross-compare cell generation across these studies.

#### **RESOURCE AVAILABILITY**

### Lead contact

Requests for further information and resources should be directed to and will be fulfilled by the lead contact, Jürgen Knoblich (juergen.knoblich@imba.

### **Materials availability**

This study did not generate unique reagents. WA01 (H1) and WA09 (H9) cell lines may be obtained from WiCell (https://www.wicell.org). SCCF-176J clone#1 (abbreviated 176), SCCF-177J clone#8 (abbreviated 177), and SCCF-178J clone#5 (abbreviated 178) iPSC lines are available via the IMBA iPSC Biobank Webshop (https://shop.vbc.ac.at/ipsc\_biobank). Human-induced pluripotent stem cell lines Rozh\_5, Uofv\_1, and Xuja\_2 are available from the HipSci consortium (https://www.hipsci.org).

### Data and code availability

- Raw single-cell and time course bulk RNA-seq data generated in this work have been deposited at the European Genome-phenome Archive (EGA), which is hosted by the EBI and the CRG, under series numbers EGA: EGAS50000000662 and EGA: EGAS50000000663, respectively. They are available under controlled access, provided by the Data Access Committee for IMBA (ethics@imba.oeaw.ac.at); see the Data Access Policy at the respective EGA entries.
- Processed single-cell and time course bulk RNA-seq data have been deposited and are publicly available on NCBI Gene Expression Omnibus (GEO) via series numbers GEO: GSE277968 and GEO: GSE277967.
- This paper analyzes existing, publicly available gene expression count matrices from Braun et al.,<sup>24</sup> accessible at https://github.com/linnarsson-lab/developing-human-brain/; from Bhaduri et al.,<sup>23</sup> accessible at The Neuroscience Multi-omic Data Archive (NeMO) (RRID: SCR\_002001) via https://data.nemoarchive.org/biccno/grant/u01\_devhu/kriegstein/transcriptome/scell/10x\_v2/human/processed/counts/; from Amin et al.,<sup>19</sup> accessible at GEO via series number GEO: GSE233574; and 3D expression maps from Fleck et al.,<sup>31</sup> accessible on Mendeley: https://doi.org/10.17632/g4xg38mwcn.2.

- R scripts and corresponding source data to reproduce all figures and tables presented in the manuscript are deposited and are publicly available on GitHub (https://github.com/jn-goe/brain\_organoids\_four\_ protocols) and Zenodo: https://doi.org/10.5281/zenodo.13742634.
- Functionalities of the NEST-Score are publicly available as R package on GitHub (https://github.com/jn-goe/NESTScore) and Zenodo: https://doi.org/10.5281/zenodo.13974434.
- The Shiny App<sup>47</sup> for data exploration is publicly available on https://vienna-brain-organoid-explorer.vbc.ac.at/.

#### **ACKNOWLEDGMENTS**

We thank all members of the Bock, von Haeseler, Esk, and Knoblich labs for technical expertise and feedback. We thank IMP/IMBA BioOptics services for expert microscopy and flow cytometry services. We thank M. Gollowitzer and the IMP/IMBA Information Technology Department for IT support. We thank A. Sommer and the VBCF NGS unit (www.viennabiocenter.org/ facilities) for consultation and sequencing. We acknowledge the IMBA Stem Cell Core facility for generation of the induced pluripotent stem cell line SCCF-176J clone#1, SCCF-177J clone#8, and SCCF-178J clone#5. Funding: J.N. and L.H. are members of the VBC PhD Program. Work in J. A.K.'s laboratory is supported by the Austrian Academy of Sciences, the Austrian Federal Ministry of Education, Science and Research, the City of Vienna, the Austrian Science Fund (Special Research Program F78 Stem Cell, F 7803-B, FWF P 35369, and project SFB-F78 P04), the HCA|Organoid project funded by the European Union's Horizon 2020 research and innovation program (grant agreement no. 874769, coordinator: C.B.), and a European Research Council (ERC) Advanced Grant under the European Union's Horizon 2020 program (695642). Work in A.v.H.'s laboratory is supported by the Austrian Science Fund (Special Research Program SFB-F78, F 7811-B) and the Research Platform SinCeReSt-Single cell regulation of stem cells. Work in C.B.'s laboratory is supported by a European Research Council (ERC) Consolidator Grant (no. 101001971) and by Austrian Science Fund (F.W.F.) Special Research Area grants (SFB F6102; SFB F7001).

### **AUTHOR CONTRIBUTIONS**

Conceptualization, J.N., M.B., A.v.H., C.E., and J.A.K.; investigation, M.B., T. K., S.L., and C.E.; methodology, J.N., M.B., L.H., and C.E.; data curation, J.N., L.H., M.N., and L.D.; formal analysis, J.N., L.H., and M.N.; software, J.N., L.H., and M.N.; visualization, J.N. and L.H.; writing—original draft: J.N. and C.E.; writing—review & editing, J.N., M.B., L.H., S.L., C.B., A.v.H., C.E., and J.A. K.; supervision, C.B., A.v.H., C.E., and J.A.K.; funding acquisition, C.B., A.v. H., C.E., and J.A.K.

### **DECLARATION OF INTERESTS**

J.A.K. is inventor on a patent describing cerebral organoid technology and cofounder and scientific advisory board member of a:head bio AG. C.B. is a cofounder and scientific advisor of Myllia Biotechnology and Neurolentech. The other authors declare no competing interests.

## DECLARATION OF GENERATIVE AI AND AI-ASSISTED TECHNOLOGIES IN THE WRITING PROCESS

During the preparation of this work some authors used ChatGPT (https://chatgpt.com) in order to improve readability of initial text drafts. After using this tool, the authors reviewed and edited the content as needed and takes full responsibility for the content of the published article.

### **STAR**\*METHODS

Detailed methods are provided in the online version of this paper and include the following:

- KEY RESOURCES TABLE
- EXPERIMENTAL MODEL AND STUDY PARTICIPANT DETAILS



- o Ethics approval and consent to participate
- METHOD DETAILS
  - o Cell culture
  - o Brain organoid generation
  - Dorsal protocol
  - o Ventral protocol
  - o Midbrain protocol
  - Striatum protocol
  - o Organoid media
  - o Brainphys
  - o scRNA-sequencing
  - o Bulk RNA-sequencing
- QUANTIFICATION AND STATISTICAL ANALYSIS
  - o scRNA-seq sample pooling and demultiplexing
  - o Pre-processing and downstream analysis
  - VoxHunt correlation analysis
  - o Measure cell neighborhood homogeneity: NEST-score
  - Module Score based on bulk RNA-seq differentially expressed marker genes
  - o Gene Ontology scores for scRNA-seq
  - o Integration of in vivo and in vitro scRNA-seq data
  - o Time course bulk RNA-seq analysis
  - o Pre-processing and downstream analysis
  - Explained variance by experimental condition
  - o Gene expression heatmaps and sample clustering
  - o Gene Ontology scores for bulk RNA-seq
  - o Protocol-specific marker genes

### SUPPLEMENTAL INFORMATION

Supplemental information can be found online at https://doi.org/10.1016/j.ceirep.2025.116168.

Received: November 7, 2024 Revised: January 22, 2025 Accepted: July 29, 2025 Published: August 26, 2025

### REFERENCES

- Eiraku, M., Watanabe, K., Matsuo-Takasaki, M., Kawada, M., Yonemura, S., Matsumura, M., Wataya, T., Nishiyama, A., Muguruma, K., and Sasai, Y. (2008). Self-Organized Formation of Polarized Cortical Tissues from ESCs and Its Active Manipulation by Extrinsic Signals. Cell Stem Cell 3, 519–532. https://doi.org/10.1016/j.stem.2008.09.002.
- Lancaster, M.A., Renner, M., Martin, C.-A., Wenzel, D., Bicknell, L.S., Hurles, M.E., Homfray, T., Penninger, J.M., Jackson, A.P., and Knoblich, J.A. (2013). Cerebral organoids model human brain development and microcephaly. Nature 501, 373–379. https://doi.org/10.1038/nature12517.
- Lancaster, M.A., and Knoblich, J.A. (2014). Organogenesis in a dish: Modeling development and disease using organoid technologies. Science 345, 1247125. https://doi.org/10.1126/science.1247125.
- Camp, J.G., Badsha, F., Florio, M., Kanton, S., Gerber, T., Wilsch-Bräuninger, M., Lewitus, E., Sykes, A., Hevers, W., Lancaster, M., et al. (2015). Human cerebral organoids recapitulate gene expression programs of fetal neocortex development. Proc. Natl. Acad. Sci. 112, 15672–15677. https://doi.org/10.1073/pnas.1520760112.
- Quadrato, G., Brown, J., and Arlotta, P. (2016). The promises and challenges of human brain organoids as models of neuropsychiatric disease. Nat. Med. 22, 1220–1228. https://doi.org/10.1038/nm.4214.
- Quadrato, G., and Arlotta, P. (2017). Present and future of modeling human brain development in 3D organoids. Curr. Opin. Cell Biol. 49, 47–52. https://doi.org/10.1016/j.ceb.2017.11.010.

- Rossi, G., Manfrin, A., and Lutolf, M.P. (2018). Progress and potential in organoid research. Nat. Rev. Genet. 19, 671–687. https://doi.org/10.1038/s41576-018-0051-9.
- Velasco, S., Kedaigle, A.J., Simmons, S.K., Nash, A., Rocha, M., Quadrato, G., Paulsen, B., Nguyen, L., Adiconis, X., Regev, A., et al. (2019). Individual brain organoids reproducibly form cell diversity of the human cerebral cortex. Nature 570, 523–527. https://doi.org/10.1038/s41586-019-1289-x.
- Arlotta, P., and Paşca, S.P. (2019). Cell diversity in the human cerebral cortex: from the embryo to brain organoids. Curr. Opin. Neurobiol. 56, 194–198. https://doi.org/10.1016/j.conb.2019.03.001.
- Kyrousi, C., and Cappello, S. (2020). Using brain organoids to study human neurodevelopment, evolution and disease. WIREs Dev. Biol. 9, e347. https://doi.org/10.1002/wdev.347.
- Kelley, K.W., and Paşca, S.P. (2022). Human brain organogenesis: Toward a cellular understanding of development and disease. Cell 185, 42–61. https://doi.org/10.1016/j.cell.2021.10.003.
- Eichmüller, O.L., and Knoblich, J.A. (2022). Human cerebral organoids a new tool for clinical neurology research. Nat. Rev. Neurol. 18, 661–680. https://doi.org/10.1038/s41582-022-00723-9.
- Arlotta, P., and Gage, F.H. (2023). Neural Organoids and the Quest to Understand and Treat Psychiatric Disease. Biol. Psychiatry 93, 588–589. https://doi.org/10.1016/j.biopsych.2023.01.021.
- Bagley, J.A., Reumann, D., Bian, S., Lévi-Strauss, J., and Knoblich, J. A. (2017). Fused cerebral organoids model interactions between brain regions. Nat. Methods 14, 743–751. https://doi.org/10.1038/nmeth. 4304
- Birey, F., Andersen, J., Makinson, C.D., Islam, S., Wei, W., Huber, N., Fan, H.C., Metzler, K.R.C., Panagiotakos, G., Thom, N., et al. (2017). Assembly of functionally integrated human forebrain spheroids. Nature 545, 54–59. https://doi.org/10.1038/nature22330.
- Mayhew, C.N., and Singhania, R. (2023). A review of protocols for brain organoids and applications for disease modeling. STAR Protoc. 4, 101860. https://doi.org/10.1016/j.xpro.2022.101860.
- Paşca, S.P. (2019). Assembling human brain organoids. Science 363, 126–127. https://doi.org/10.1126/science.aau5729.
- Reumann, D., Krauditsch, C., Novatchkova, M., Sozzi, E., Wong, S.N., Zabolocki, M., Priouret, M., Doleschall, B., Ritzau-Reid, K.I., Piber, M., et al. (2023). In vitro modeling of the human dopaminergic system using spatially arranged ventral midbrain-striatum-cortex assembloids. Nat. Methods 20, 2034–2047. https://doi.org/10.1038/s41592-023-
- Amin, N.D., Kelley, K.W., Kaganovsky, K., Onesto, M., Hao, J., Miura, Y., McQueen, J.P., Reis, N., Narazaki, G., Li, T., et al. (2024). Generating human neural diversity with a multiplexed morphogen screen in organoids. Cell Stem Cell 31, 1831–1846.e9. https://doi.org/10.1016/j.stem.2024.
- Kanton, S., Boyle, M.J., He, Z., Santel, M., Weigert, A., Sanchís-Calleja, F., Guijarro, P., Sidow, L., Fleck, J.S., Han, D., et al. (2019). Organoid single-cell genomic atlas uncovers human-specific features of brain development. Nature 574, 418–422. https://doi.org/10.1038/s41586-019-1654-9.
- Sanchís-Calleja, F., Jain, A., He, Z., Okamoto, R., Rusimbi, C., Rifes, P., Rathore, G.S., Santel, M., Janssens, J., Seimiya, M., et al. (2024). Decoding morphogen patterning of human neural organoids with a multiplexed single-cell transcriptomic screen. preprint at bioRxiv. https://doi.org/10.1101/2024.02.08.579413.
- He, Z., Dony, L., Fleck, J.S., Szałata, A., Li, K.X., Slišković, I., Lin, H.-C., Santel, M., Atamian, A., Quadrato, G., et al. (2024). An integrated transcriptomic cell atlas of human neural organoids. Nature 635, 690–698. https://doi.org/10.1038/s41586-024-08172-8.
- Bhaduri, A., Sandoval-Espinosa, C., Otero-Garcia, M., Oh, I., Yin, R., Eze, U.
   C., Nowakowski, T.J., and Kriegstein, A.R. (2021). An atlas of cortical

### Resource



- arealization identifies dynamic molecular signatures. Nature 598, 200–204. https://doi.org/10.1038/s41586-021-03910-8.
- Braun, E., Danan-Gotthold, M., Borm, L.E., Lee, K.W., Vinsland, E., Lönnerberg, P., Hu, L., Li, X., He, X., Andrusivová, Ž., et al. (2023). Comprehensive cell atlas of the first-trimester developing human brain. Science 382, eadf1226. https://doi.org/10.1126/science.adf1226.
- Eichmüller, O.L., Corsini, N.S., Vértesy, Á., Morassut, I., Scholl, T., Gruber, V.-E., Peer, A.M., Chu, J., Novatchkova, M., Hainfellner, J.A., et al. (2022).
   Amplification of human interneuron progenitors promotes brain tumors and neurological defects. Science 375, eabf5546. https://doi.org/10.1126/science.abf5546.
- Martins-Costa, C., Pham, V.A., Sidhaye, J., Novatchkova, M., Wiegers, A., Peer, A., Möseneder, P., Corsini, N.S., and Knoblich, J.A. (2023). Morphogenesis and development of human telencephalic organoids in the absence and presence of exogenous extracellular matrix. EMBO J. 42, e113213. https://doi.org/10.15252/embj.2022113213.
- Uzquiano, A., Kedaigle, A.J., Pigoni, M., Paulsen, B., Adiconis, X., Kim, K., Faits, T., Nagaraja, S., Antón-Bolaños, N., Gerhardinger, C., et al. (2022). Proper acquisition of cell class identity in organoids allows definition of fate specification programs of the human cerebral cortex. Cell 185, 3770–3788.e27. https://doi.org/10.1016/j.cell.2022.09.010.
- Heumos, L., Schaar, A.C., Lance, C., Litinetskaya, A., Drost, F., Zappia, L., Lücken, M.D., Strobl, D.C., Henao, J., Curion, F., et al. (2023). Best practices for single-cell analysis across modalities. Nat. Rev. Genet. 24, 550–572. https://doi.org/10.1038/s41576-023-00586-w.
- Fleck, J.S., Sanchís-Calleja, F., He, Z., Santel, M., Boyle, M.J., Camp, J. G., and Treutlein, B. (2021). Resolving organoid brain region identities by mapping single-cell genomic data to reference atlases. Cell Stem Cell 28, 1148–1159.e8. https://doi.org/10.1016/j.stem.2021.02.015.
- Thompson, C.L., Ng, L., Menon, V., Martinez, S., Lee, C.-K., Glattfelder, K., Sunkin, S.M., Henry, A., Lau, C., Dang, C., et al. (2014). A High-Resolution Spatiotemporal Atlas of Gene Expression of the Developing Mouse Brain. Neuron 83, 309–323. https://doi.org/10.1016/j.neuron. 2014 05 033
- Fleck, J.S. (2020). VoxHunt Expression Maps. Version 2 (Mendeley Data). https://doi.org/10.17632/g4xg38mwcn.2.
- 32. Kullback, S., and Leibler, R.A. (1951). On Information and Sufficiency. Ann. Math. Statist. 22. 79–86.
- Giandomenico, S.L., Sutcliffe, M., and Lancaster, M.A. (2021). Generation and long-term culture of advanced cerebral organoids for studying later stages of neural development. Nat. Protoc. 16, 579–602. https://doi.org/ 10.1038/s41596-020-00433-w.
- Stuart, T., Butler, A., Hoffman, P., Hafemeister, C., Papalexi, E., Mauck, W. M., Hao, Y., Stoeckius, M., Smibert, P., and Satija, R. (2019). Comprehensive Integration of Single-Cell Data. Cell 177, 1888–1902.e21. https://doi.org/10.1016/j.cell.2019.05.031.
- Ritchie, M.E., Phipson, B., Wu, D., Hu, Y., Law, C.W., Shi, W., and Smyth, G.K. (2015). limma powers differential expression analyses for RNAsequencing and microarray studies. Nucleic Acids Res. 43, e47. https:// doi.org/10.1093/nar/gkv007.
- Hoffman, G.E., and Schadt, E.E. (2016). variancePartition: interpreting drivers of variation in complex gene expression studies. BMC Bioinf. 17, 483. https://doi.org/10.1186/s12859-016-1323-z.
- Strano, A., Tuck, E., Stubbs, V.E., and Livesey, F.J. (2020). Variable Outcomes in Neural Differentiation of Human PSCs Arise from Intrinsic Differences in Developmental Signaling Pathways. Cell Rep. 31, 107732. https://doi.org/10.1016/j.celrep.2020.107732.
- Kim, T.W., Piao, J., Koo, S.Y., Kriks, S., Chung, S.Y., Betel, D., Socci, N.D., Choi, S.J., Zabierowski, S., Dubose, B.N., et al. (2021). Biphasic Activation of WNT Signaling Facilitates the Derivation of Midbrain Dopamine Neurons from hESCs for Translational Use. Cell Stem Cell 28, 343–355.e5. https:// doi.org/10.1016/j.stem.2021.01.005.

- Bhaduri, A., Andrews, M.G., Mancia Leon, W., Jung, D., Shin, D., Allen, D., Jung, D., Schmunk, G., Haeussler, M., Salma, J., et al. (2020). Cell stress in cortical organoids impairs molecular subtype specification. Nature 578, 142–148. https://doi.org/10.1038/s41586-020-1962-0.
- Gordon, A., Yoon, S.-J., Tran, S.S., Makinson, C.D., Park, J.Y., Andersen, J., Valencia, A.M., Horvath, S., Xiao, X., Huguenard, J.R., et al. (2021). Long Term Maturation of Human Cortical Organoids Matches Key Early Postnatal Transitions. Nat. Neurosci. 24, 331–342. https://doi.org/10. 1038/s41593-021-00802-y.
- Vértesy, Á., Eichmüller, O.L., Naas, J., Novatchkova, M., Esk, C., Balmaña, M., Ladstaetter, S., Bock, C., von Haeseler, A., and Knoblich, J.A. (2022). Gruffi: an algorithm for computational removal of stressed cells from brain organoid transcriptomic datasets. EMBO J. 41, e111118. https://doi.org/ 10.15252/embj.2022111118.
- Qian, X., Song, H., and Ming, G.L. (2019). Brain organoids: advances, applications and challenges. Development 146, dev166074. https://doi.org/10.1242/dev.166074.
- Gene Ontology Consortium; Aleksander, S.A., Balhoff, J., Carbon, S., Cherry, J.M., Drabkin, H.J., Ebert, D., Feuermann, M., Gaudet, P., Harris, N.L., et al. (2023). The Gene Ontology knowledgebase in 2023. Genetics 224, iyad031. https://doi.org/10.1093/genetics/iyad031.
- Esk, C., Lindenhofer, D., Haendeler, S., Wester, R.A., Pflug, F., Schroeder, B., Bagley, J.A., Elling, U., Zuber, J., von Haeseler, A., and Knoblich, J.A. (2020). A human tissue screen identifies a regulator of ER secretion as a brain-size determinant. Science 370, 935–941. https://doi.org/10.1126/ science.abb5390.
- Fleck, J.S., Jansen, S.M.J., Wollny, D., Zenk, F., Seimiya, M., Jain, A., Okamoto, R., Santel, M., He, Z., Camp, J.G., and Treutlein, B. (2023). Inferring and perturbing cell fate regulomes in human brain organoids. Nature 621, 365–372. https://doi.org/10.1038/s41586-022-05279-8.
- Fedele, S., Collo, G., Behr, K., Bischofberger, J., Müller, S., Kunath, T., Christensen, K., Gündner, A.L., Graf, M., Jagasia, R., and Taylor, V. (2017). Expansion of human midbrain floor plate progenitors from induced pluripotent stem cells increases dopaminergic neuron differentiation potential. Sci. Rep. 7, 6036. https://doi.org/10.1038/s41598-017-05633-1
- Chang, W., Cheng, J., Allaire, J., Sievert, C., Schloerke, B., Xie, Y., Allen, J., McPherson, J., Dipert, A., and Borges, B. (2024). shiny: Web Application Framework for R. Version R package version 1.9.1. https://CRAN.Rproject.org/package=shiny.
- Yoon, S.-J., Elahi, L.S., Paşca, A.M., Marton, R.M., Gordon, A., Revah, O., Miura, Y., Walczak, E.M., Holdgate, G.M., Fan, H.C., et al. (2019). Reliability of human cortical organoid generation. Nat. Methods 16, 75–78. https://doi.org/10.1038/s41592-018-0255-0.
- Büttner, M., Miao, Z., Wolf, F.A., Teichmann, S.A., and Theis, F.J. (2019). A test metric for assessing single-cell RNA-seq batch correction. Nat. Methods 16, 43–49. https://doi.org/10.1038/s41592-018-0254-1.
- Wimmer, R.A., Leopoldi, A., Aichinger, M., Wick, N., Hantusch, B., Novatchkova, M., Taubenschmid, J., Hämmerle, M., Esk, C., Bagley, J.A., et al. (2019). Human blood vessel organoids as a model of diabetic vasculopathy. Nature 565, 505–510. https://doi.org/10.1038/s41586-018-0858-8.
- Atamian, A., Birtele, M., Hosseini, N., Nguyen, T., Seth, A., Del Dosso, A., Paul, S., Tedeschi, N., Taylor, R., Coba, M.P., et al. (2024). Human cerebellar organoids with functional Purkinje cells. Cell Stem Cell 31, 39–51. e6. https://doi.org/10.1016/j.stem.2023.11.013.
- Langmead, B., and Salzberg, S.L. (2012). Fast gapped-read alignment with Bowtie 2. Nat. Methods 9, 357–359. https://doi.org/10.1038/nmeth. 1923
- Heaton, H., Talman, A.M., Knights, A., Imaz, M., Gaffney, D.J., Durbin, R., Hemberg, M., and Lawniczak, M.K.N. (2020). Souporcell: robust clustering of single-cell RNA-seq data by genotype without reference genotypes. Nat. Methods 17, 615–620. https://doi.org/10.1038/s41592-020-0820-1.





- Hao, Y., Stuart, T., Kowalski, M.H., Choudhary, S., Hoffman, P., Hartman, A., Srivastava, A., Molla, G., Madad, S., Fernandez-Granda, C., and Satija, R. (2024). Dictionary learning for integrative, multimodal and scalable single-cell analysis. Nat. Biotechnol. 42, 293–304. https://doi.org/10.1038/ s41587-023-01767-y.
- Wolock, S.L., Lopez, R., and Klein, A.M. (2019). Scrublet: Computational Identification of Cell Doublets in Single-Cell Transcriptomic Data. Cell Syst. 8, 281–291.e9. https://doi.org/10.1016/j.cels.2018.11.005.
- Love, M.I., Huber, W., and Anders, S. (2014). Moderated estimation of fold change and dispersion for RNA-seq data with DESeq2. Genome Biol. 15, 550. https://doi.org/10.1186/s13059-014-0550-8.
- Tirosh, I., Izar, B., Prakadan, S.M., Wadsworth, M.H., Treacy, D., Trombetta, J.J., Rotem, A., Rodman, C., Lian, C., Murphy, G., et al. (2016). Dissecting the multicellular ecosystem of metastatic melanoma by single-cell RNA-seq. Science 352, 189–196. https://doi.org/10.1126/science.aad0501.



### **STAR**\*METHODS

### **KEY RESOURCES TABLE**

REAGENT or RESOURCE	SOURCE	IDENTIFIER
Chemicals, peptides, and recombinant proteins		
Essential 8 Medium	Thermo Fisher Scientific	cat. no. A1517001
/itronectin	Stem Cell Technologies	cat. no. 100-0763
OPBS -/-	Gibco	cat. no. 14190-250
Accutase	Sigma-Aldich	cat. no. A6964
RevitaCell	Thermo Fisher Scientific	cat. no. A2644501
96-well ultra-low-attachment U-bottom plate	Sigma-Aldich	cat. no. CLS7007
Matrigel	Corning	cat. no. 356235
CHIR	Merck	cat. no. 361571
BDNF	Stemcell Technologies	cat. no. 78005.3
GDNF	Stemcell Technologies	cat. no. 78057.3
db-cAMP	Santa Cruz Biotechnology	cat. no. sc-201567C
SAG	Merck	cat. no. US1566660
WP-2	Sigma-Aldich	cat. no. 10536
Noggin	R&D Systems	cat. no. 6057
SB431542	Stemgent	cat. no. 04-0010-10
FGF-8	R&D Systems	cat. no. 5057-FF
DMEM/F12	Invitrogen	cat. no. 11330-057
N2 Supplement	Thermo Fisher Scientific	cat. no. 17502001
GlutaMAX-I	Thermo Fisher Scientific	cat. no. 35050-038
MEM-NEAA	Sigma-Aldrich	cat. no. M7145
Heparin	Sigma-Aldrich	cat. no. H3149
PenStrep	Sigma-Aldrich	cat. no. P4333
Neurobasal	Gibco	cat. no. 21103049
327–A	Thermo Fisher Scientific	cat. no. 12587010
nsulin	Sigma-Aldrich	cat. no. 19278
Antibiotic-Antimycotic	Thermo Fisher Scientific	cat. no. 15240062
327 + A	Thermo Fisher Scientific	cat. no. 17504044
/itamin C	Sigma-Aldrich	cat. no. A4544
sodium bicarbonate	Sigma-Aldrich	cat. no. S5761
BrainPhys	Stemcell Technologies	cat. no. 05790
CD Lipid Concentrate	Thermo Fisher Scientific	cat. no. 11905031
10x Trypsin	Gibco	cat. no. 15400
FurboDNase	Thermo Fisher Scientific	cat. no. AM2238
BSA	Biostatus	cat. no. DR70250
「otalSeq <sup>™</sup> -A antibodies	Biolegend	cat. no. 399907
Buffer RLT	Qiagen	cat. no. 79216
Critical commercial assays		
Quantseq sequencing kit	Lexogen	cat. no. 015.384
Quantseq UMI kit	Lexogen	cat. no. 081.96
Deposited data		
raw organoid in vitro single-cell RNA-seq data	This paper	EGA: EGAS50000000662
aw organoid in vitro time-course bulk RNA-seq data	This paper	EGA: EGAS50000000663
processed organoid in vitro single-cell RNA-seq data	This paper	GEO: GSE277968

(Continued on next page)





Continued		
REAGENT or RESOURCE	SOURCE	IDENTIFIER
processed organoid <i>in vitro</i> time-course bulk RNA-seq data	This paper	GEO: GSE277967
processed human in vivo single-cell RNA-seq data	Braun et al. <sup>24</sup>	https://github.com/linnarsson-lab/ developing-human-brain/
processed human <i>in vivo</i> single-cell RNA-seq data	Bhaduri et al. <sup>23</sup>	NeMO (RRID: SCR_002001), https://data.nemoarchive.org/biccn/grant/ u01_devhu/kriegstein/transcriptome/ scell/10x_v2/human/processed/counts/
processed organoid in vitro single-cell RNA-seq data	Amin et al. <sup>19</sup>	GEO: GSE233574
orocessed mouse <i>in vivo</i> 3D expression maps (Allen Developing Mouse Brain Atlas)	Fleck et al. <sup>31</sup>	Mendeley: https://doi.org/ 10.17632/g4xg38mwcn.2
Experimental models: Cell lines		
Human: H1: embryonic stem cell (hESCs) line WA01	WiCell	hESCs line WA01
Human: H9: embryonic stem cell (hESCs) line WA09	WiCell	hESCs line WA09
Human: Rozh_5: induced pluripotent stem cell (HipSci) line HPSl0114i-rozh_5 (ECACC 77650043)	HipSci consortium	cat. no. 77650043
Human: Xuja_2: induced pluripotent stem cell (HipSci) line HPSI1213i-xuja_2 (ECACC 77650087)	HipSci consortium	cat. no. 77650087
Human: Uofv_1: induced pluripotent stem cell (HipSci) line HPSI1113i-uofv_1 (ECACC 77650078)	HipSci consortium	cat. no. 77650078
Human: 176: induced pluripotent stem cell (HipSci) line SCCF-176J clone#1 (Ethics Approval Number EK 1596/2017)	IMBA iPSC Biobank Webshop	HipSci line SCCF-176J clone#1
Human: 177: induced pluripotent stem cell (HipSci) line SCCF-177J clone#8 (Ethics Approval Number EK 1596/2017)	IMBA iPSC Biobank Webshop	HipSci line SCCF-177J clone#8
Human: 178: induced pluripotent stem cell (HipSci) line SCCF-178J clone#5 (Ethics Approval Number EK 1596/2017)	IMBA iPSC Biobank Webshop	HipSci line SCCF-178J clone#5
Software and algorithms		
Cell Ranger (v3.0.2)	10X Genomics	https://www.10xgenomics.com/ support/software/cell-ranger
Bowtie (v2.3.4.1)	Langmead et al. <sup>52</sup>	https://github.com/BenLangmead/bowtie2
Souporcell (V2.4)	Heaton et al. <sup>53</sup>	https://github.com/wheaton5/souporcell
R (version 4.4.0)	The R Foundation for Statistical Computing	https://cran.r-project.org
Seurat (v5.0.1)	Hao et al. <sup>54</sup>	https://cran.r-project.org/package=Seurat
scrublet (v0.2.3)	Wolock et al.55	https://github.com/swolock/scrublet
/oxHunt (v1.1.0)	Fleck et al. <sup>29</sup>	https://github.com/quadbio/VoxHunt
NEST-Score (v.1.0.0)	This paper	https://github.com/jn-goe/NESTScore; Zenodo: https://doi.org/10.5281/zenodo.13974434
imma (v3.60.0)	Ritchie et al. <sup>35</sup>	https://bioconductor.org/packages/ release/bioc/html/limma.html
variancePartition (v1.34.0)	Hoffman et al. <sup>36</sup>	https://bioconductor.org/packages/ release/bioc/html/variancePartition.html
DESeq2 (v1.44.0)	Love et al. <sup>56</sup>	https://www.bioconductor.org/packages/release/bioc/html/DESeq2.html
shiny (v1.9.1)	Chang et al.47	https://cran.r-project.org/package=shiny
Brain Organoid Explorer	This paper	https://vienna-brain-organoid-explorer.vbc.ac.at
Other		
Source data and scripts related to the analysis of brain organoid transcriptomic data (v2)	This paper	https://github.com/jn-goe/ brain_organoids_four_protocols; Zenodo: https://doi.org/10.5281/zenodo.13742634

### Resource



### **EXPERIMENTAL MODEL AND STUDY PARTICIPANT DETAILS**

### Ethics approval and consent to participate

The study was approved by the local institutional review board (IRB) of the Medical University of Vienna EK 1596/2017. Informed consent from donors providing material for iPSC generation (IMBA iPSC biobank, see below) was obtained from patients and/or their legal representatives.

### **METHOD DETAILS**

#### **Cell culture**

Human embryonic stem cell (hESCs) lines WA01 (H1, male) and WA09 (H9, female) were obtained from WiCell (https://www.wicell.org). Human induced pluripotent stem cell lines SCCF-176J clone#1 (abbreviated 176, female), SCCF-177J clone#8 (abbreviated 177, female) and SCCF-178J clone#5 (abbreviated 178, male) were obtained from IMBA iPSC biobank (https://shop.vbc.ac.at/ipsc\_biobank/). Human induced pluripotent stem cell lines HPSI0114i-rozh\_5 (abbreviated Rozh\_5, female, cat. no. 77650043), HPSI1113i-uofv\_1 (abbreviated Uofv\_1, male, cat. no. 77650078) and HPSI1213i-xuja\_2 (abbreviated Xuja\_2, female, cat. no. 77650087) were obtained from the HipSci consortium (https://www.hipsci.org). All lines were contamination free, STR verified and regularly tested for mycoplasma. Cell lines were maintained according to HipSci recommendations on Vitronectin (Stem Cell Technologies, cat. no. 100–0763) coated plates with Essential 8 Medium (Thermo Fisher Scientific, cat. no. A1517001 or produced inhouse). All cells were maintained in a 5% CO<sub>2</sub> incubator at 37°C. Cells were either split using DPBS -/- (Gibco, cat. no. 14190-250) or Accutase (Sigma, cat. no. A6964) and plated in Essential 8 Medium supplemented with RevitaCell Supplement (Thermo Fisher Scientific, cat. no. A2644501).

### **Brain organoid generation**

Brain organoids were generated as previously described. <sup>18,26</sup> Media compositions are given below. Pluripotent cells were grown to 60–80% confluency and single cell suspensions were obtained using Accutase. Pelleted cells were resuspended in E8 media supplemented with RevitaCell and counted. 8 000–10 000 cells were seeded to form embryoid bodies in a 96-well ultra-low-attachment U-bottom plate (Sigma, cat. no. CLS7007).

### **Dorsal protocol**

Day 0: Seeding in 150  $\mu$ L E8 supplemented with RevitaCell. Day 3: E8 media. Days 6, 7, 8, 9: Neural induction media (NI), Day 10: 1% Matrigel in NI media (Corning, cat. no. 356235) and transfer to 10 cm plates coated with anti-adherence rinsing solution (Stemcell Technologies, cat. no. 07010). Day 13, 14: NI media supplemented with 3 mM CHIR (Merck, cat. no. 361571), Days 16, 19, 22: Improved-A media with transfer to shaker on day 19. Days 25–40 every 3–4 days: Improved+A media. Days 40–60 every 3–4 days: Improved+A media supplemented with 1% Matrigel, Day 62: 75% Improved+A media mixed with 25% Brainphys media supplemented with 1% Matrigel. Day 65: 50% Improved+A media mixed with 50% Brainphys media supplemented with 1% Matrigel. Days 72–120 every 3–4 days: Brainphys media supplemented with 1% Matrigel, 20 ng mL $^{-1}$  BDNF (Stemcell Technologies, cat. no. 78005.3), 20 ng mL $^{-1}$  GDNF (Stemcell Technologies, cat. no. sc-201567C).

### **Ventral protocol**

Day 0: Seeding in 150  $\mu$ L E8 supplemented with RevitaCell. Day 3: E8 media. Days 5, 7, 9, 10: Neural induction media (NI) supplemented with 100 nM SAG (Merck, cat. no. US1566660) and 2.5  $\mu$ M IWP-2 (Sigma-Aldrich, cat. no. 10536) with 1% Matrigel added at day 10. Days 13, 15, 17: Improved-A supplemented with 100 nM SAG and 2.5  $\mu$ M IWP-2. Organoid maturation from day 19 on as in dorsal protocol.

### Midbrain protocol

Days 0, 2:150  $\mu$ L NI supplemented with RevitaCell, 200 ng mL $^{-1}$  Noggin (R&D Systems, cat. no. 6057), 10  $\mu$ M SB431542 (Stemgent, cat. no. 04-0010-10) and 0.8  $\mu$ M CHIR. Day 4: NI supplemented with 200 ng mL $^{-1}$  Noggin, 10  $\mu$ M SB431542, 0.8  $\mu$ M CHIR, 300 nM SAG and 100 ng mL $^{-1}$  FGF-8 (fibroblast growth factor 8; R&D Systems, cat. no. 5057-FF). Day 6: NI supplemented with 300 nM SAG and 100 ng mL $^{-1}$  FGF-8. Day 8: Improved-A supplemented with 300 nM SAG, 100 ng mL $^{-1}$  FGF-8, 2% Matrigel. Transfer to a 10cm dish. Day 10: Improved-A supplemented with 2% Matrigel. Day 13: Improved-A. Days 16–25 every 3–4 days: Improved+A media. Organoid maturation from day 25 on as in dorsal protocol.

### Striatum protocol

Days 0, 2:150 µL NI supplemented with RevitaCell, 10 nM SAG, 2.5 µM IWP-2. Day 4: NI supplemented with 10 nM SAG, 2.5 µM IWP-2. Day 6: NI, Day 8: Day 8: Improved-A supplemented with 2% Matrigel. Transfer to a 10cm dish. Day 10: Improved-A supplemented with 2% Matrigel. Day 13: Improved-A. Days 16–25 every 3–4 days: Improved+A media. Organoid maturation from day 25 on as in dorsal protocol.





#### **Organoid** media

### Neural induction medium (NI)

DMEM/F12 (Invitrogen, cat. no. 11330-057), 1% N2 Supplement (Thermo Fisher, cat. no. 17502001), 1% GlutaMAX-I (Thermo Fisher, cat. no. 35050-038), 1% MEM-NEAA (Sigma-Aldrich, M7145), 1:1000 heparin solution (Sigma-Aldrich, cat. no. H3149-100KU), 1% PenStrep (Sigma-Aldrich, cat. no. P4333).

#### Improved-A medium

50:50 DMEM/F12: Neurobasal (Gibco, cat. no. 21103049), 0.5% N2 supplement, 2% B27-A (Thermo Fisher, cat. no. 12587010), 1:4000 insulin (Sigma-Aldrich, cat. no. 19278), 1% GlutaMAX, 0.5% MEM-NEAA, 1% Antibiotic-Antimycotic (Thermo Fisher, cat. no. 15240062).

### Improved+A medium

50:50 DMEM/F12: Neurobasal. 0.5% N2 Supplement, 2% B27 + A (Thermo Fisher, cat. no. 17504044), 1:4000 insulin, 1% GlutaMAX, 0.5% MEM-NEAA, 1% Antibiotic-Antimycotic, 1% vitamin C solution (40 mM stock in DMEM/F12) (Vitamin C: Sigma-Aldrich, cat. no. A4544),  $1\ g\ L^{-1}$  sodium bicarbonate (Sigma-Aldrich, cat. no. S5761).

### **Brainphys**

BrainPhys Neuronal Medium (Stemcell Technologies, cat. no. 05790), 2% B27 + A, 1% N2 Supplement, 1% CD Lipid Concentrate (Thermo Fisher Scientific, cat. no.11905031), 1% Antibiotic-Antimycotic, 1:147 20% glucose solution.

### scRNA-sequencing

Organoids were dissociated at day 120 by incubation in a 9:1 mixture of Accutase (Sigma Aldrich, cat. no. A6954) and 10x Trypsin (Gibco, cat. no. 15400) at 37°C on a Thermo-shaker (800 rpm) for approximately two hours and four units of TurboDNase (Thermo cat. no. AM2238) were added after 30 min. After enzymatic dissociation, cells were filtered through a 35 µm strainer followed by dilution with 1% BSA in DPBS—/— (Biostatus; cat. no. DR70250, 0.3 mM), counted and labeled (hashed) with TotalSeq-A antibodies (Biolegend) as required to allow demultiplexing of 4 samples either by genetic background or hash information per single cell transcriptomic reaction. For hashing, cells were stained for 30 min on ice, washed twice with 1% BSA in DPBS—/—. After flow cytometry sorting a pool of equal cell numbers for each of the 4 samples was used as input for the Chromium Next GEM Single Cell 3′ Gene Expression (v3.1) following the 10x Genomics user guide (one experiment of H9 cells in the ventral condition and one sample in 177, dorsal condition failed leading to only three cell lines being loaded in these instances). Sequencing of gene expression and hash libraries was performed on an Illumina NovaSeq S4 lane.

### **Bulk RNA-sequencing**

RNA samples were extracted from organoids collected in Buffer RLT (Qiagen, cat. no. 79216) using the RNA isolation kit provided by VBC core facilities. The kit uses carboxylate-modified Sear-Mag Speed beads and was applied using the Kingfisher instrument (Thermo). For RNA sequencing Lexogen's Quantseq kit was used, including the UMI extension (Lexogen, cat. no. 015.384, 081.96). Sequencing was performed on Illumina NextSeq High Output 75 cycle lanes and Illumina Novaseq S1 100 cycle lanes and reads combined. All kits were used according to manufacturers' instructions. Samples were collected at crucial times during protocols (days 13, 25, 40, 80, 120 for dorsal and ventral, and days 16, 40, 80, 120 for midbrain and striatum).

### **QUANTIFICATION AND STATISTICAL ANALYSIS**

### scRNA-seq sample pooling and demultiplexing

Sequencing data of 10X libraries was processed using Cell Ranger software (v3.0.2, 10X Genomics) using reference genome GRCh38. Cells were demultiplexed by cell line genotype using Souporcell (v2.4)<sup>53</sup> and two replicate organoids per cell line and protocol pooled for analysis. In experiments containing hash information, hash information was used for demultiplexing.

### **Pre-processing and downstream analysis**

Per sample resulting cell-by-gene, unique molecular identifier (UMI) count matrices were analyzed in R (v4.4.0) using Seurat<sup>54</sup> (v5.0.1). We observed high cell-wise expression levels of MALAT1 which is known to be a non-informative sequencing artifact in scRNA-seq data, dominating total number of UMIs in some cells and influencing gene expression normalization and subsequent downstream analysis. Hence, we discarded cells, in which more than 10% of all UMIs were assigned to only one gene and subsequently deleted MALAT1 from the count matrices of all *in vitro* datasets. Then, we filtered for high-quality cells based on doublet detection performed with Python Package scrublet<sup>55</sup> (v0.2.3, loaded via R Package reticulate (v1.38.0)), number of uniquely detected genes ('nFeature') between 500 and 5,000, number of UMIs ('nCount') between 500 and 10,000, percentage of mitochondrial reads between 0.1% and 15% and percentage of ribosomal reads between 0.1% and 50%.

Counts across all replicates, cell lines and protocols were merged, and genes expressed in less than 10 cells were discarded. After cell-wise count log-normalization ('LogNormalize'), 3,000 highly variable genes were identified ('FindVariableFeatures') and ribosomal and mitochondrial genes were removed from the list of highly variable genes. Next, we performed cell-wise cell cycle annotation by Seurat's function 'CellCycleScoring' and gene list 'cc.gene'. Data was scaled ('ScaleData') whilst regressing out cell cycle

### Resource



biases (vars.to.regress = c('S.Score', 'G2M.Score') and Principal Component Analysis was performed ('RunPCA'). The shared nearest neighbor graph ('FindNeighbors') and the Louvain clustering algorithm ('FindClusters', with resolution 3.5) as well as the UMAP embedding ('RunUMAP') were computed on the first 40 Principal Components. 40 Principal Components were chosen due to flattening of an Elbow Plot showing explained variance against number of Principal Components and because well-known clusters and differentiation trajectories became apparent in the subsequent UMAP visualization. Positively differentially expressed genes per cluster were identified using Seurat's function 'FindAllMarkers' (using the default Wilcoxon Rank-Sum test) and genes were retained based on an average log fold change larger than 1 and an adjusted *p*-value below 0.01 (by default Bonferroni corrected; Table S1). Clusters were annotated based on expression of marker genes and hierarchically aggregated to a coarser cell type annotation (Table S2).

### **VoxHunt correlation analysis**

For comparison of the scRNA-seq organoid data with spatial gene expression data on a mouse brain slice (Allen Developing Mouse Brain Atlas<sup>30</sup>), we used VoxHunt<sup>29</sup> (v1.1.0) and the provided sample of embryonic day 13 ('E13').<sup>31</sup> For the Spearman correlation analysis with subsets of the scRNA-seq organoid atlas, we pooled the top 15 (based on the provided Area under the Curve value, AUC) genes based on the sample's respective annotation level 'custom\_2' using VoxHunt's function 'structure\_markers'.

### Measure cell neighborhood homogeneity: NEST-score

The NEST-Score was computed for each protocol separately, hence for one protocol, the data was subset to all cells generated in this specific protocol. The concept of the NEST-Score will be explained with respect to the 8 different cell lines that contribute to the dorsal, midbrain and striatum protocol. For the ventral protocol, only 7 contributing cell lines are present, and the different number of cell lines results in a different range of NEST-Scores as can be seen in Figure 2B.

For each subset, downstream analysis was re-computed with Seurat, in more detail, the computation of the most variable 2,000 features ('FindVariableFeatures'), data scaling ('ScaleData'), Principal Component Analysis ('RunPCA') and nearest neighbor search ('FindNeighbors', based on Euclidean distance in the space spanned by the first 40 Principal Components).

Subsequently, for a cell i and its k nearest neighbors  $N_i^k$ , we count how often each cell line x occurs. The resulting 8-dimensional vector (since 8 cell lines are considered) is then divided by k to obtain the local cell line distribution

$$f_i^{local}(x) = \frac{\left| N_i^k \cap L_x \right|}{k}$$

for cell i and cell line x, where  $L_x$  is the set of all cells from cell line x. The local cell line distribution vector  $f_i^{local}$  is then entry-wise divided by the global cell line distribution vector  $f_i^{global}$ , i.e., the vector of relative frequencies of cell lines across all cells within the considered protocol:

$$f^{global}(x) = \frac{|L_x|}{M},$$

where  $M = \sum_{x} |L_x|$  is the number of all cells in the considered protocol. This yields the scaled local cell line distribution

$$f_i^{scaled}(x) = c \cdot \frac{f_i^{local}(x)}{f^{global}(x)}$$
 for cell  $i$  and cell line  $x$ ,

where c is a constant such that  $\sum_{x \in L_x} f_i^{scaled}(x) = 1$ .

Finally, the NEST-Score N(i) for cell i is defined as negative Kullback-Leibler divergence<sup>32</sup> of  $f_i^{scaled}$  and the 8-dimensional uniform frequency vector  $f_i^{uniform} = (\frac{1}{8}, \dots, \frac{1}{8})$ :

$$N(i) = -D_{\mathit{KL}}\left(f_i^{\mathit{scaled}} \middle\| f^{\mathit{uniform}}\right) = -\left(\sum_{x \in \mathit{cell lines}} f_i^{\mathit{scaled}}(x) \log\left(\frac{f_i^{\mathit{scaled}}(x)}{f^{\mathit{uniform}}(x)}\right)\right),$$

for cell i.

The minus provides a more intuitive interpretation: In case the neighborhood of a cell is perfectly resembled by all considered cell lines, the local cell line distribution coincides with the global cell line distribution, yielding  $\frac{f_i^{local}(x)}{f_i^{global}(x)} = 1$  for all cell lines x. Accordingly,  $f_i^{scaled}$  becomes a uniform distribution and hence also  $\frac{f_i^{scaled}(x)}{f_i^{uniform}(x)} = 1$  for all cell lines x. Since  $log\left(\frac{f_i^{scaled}(x)}{f_i^{uniform}(x)}\right) = log(1) = 0$ , the NEST-Score reaches its upper bound '0' in this scenario. In our application we interpret this as the expression state of (and around) cell i is produced by multiple cell lines and hence consistently recovered in the considered protocol.

To binarily classify a cell as either protocol-driven (=well-mixed neighborhood with respect to cell line abundances) or cell line-driven, we computed a NEST-Score threshold as following: As a minimum requirement to identify a cell state as protocol-driven, we want to observe at least three different cell lines in the respective cell's neighborhood. Hence, we compute the NEST-Score





for an artificial scaled local cell line distribution  $f_i^{scaled}$ , which would appear if a cell's neighborhood would only consist of two cell lines with equal frequencies, i.e.,

$$f_i^{scaled} = \left(\frac{1}{2}, \frac{1}{2}, 0, \dots, 0\right).$$

For the eight cell lines (in dorsal, midbrain and striatum protocol), this results in the threshold of  $-D_{KL}(f_i^{scaled}||f^{uniform}) = -2$ . Since only 7 cell lines contribute to the ventral protocol, the threshold computation results in a value of around -1.8. A cell is then classified as protocol-driven, as soon as its NEST-Score is strictly greater than the protocol-specific threshold.

For all presented analysis, we choose k = 100 neighbors, since we observe a decreasing NEST-Score for  $k \in \{1, ..., 99\}$  and a more or less constant NEST-Score for  $k \in \{100, ..., 200\}$ . This is shown in Figure S2A for the dorsal protocol, where we compute the NEST-Scores across multiple  $k \in \{1, ..., 200\}$  for each cell, resulting in cell-wise NEST-Score lines. Those lines are colored according to our binary assignment of cells as cell line- or protocol-driven based using k = 100 and the above introduced NEST-Score threshold of k = 100 and the above introduced NEST-Score threshold of k = 100 and the above introduced NEST-Score

For the analysis of mixedness between *in vivo* and *in vitro* datasets, we consider the two sample conditions *in vivo* and *in vitro* instead of different cell lines. Again, the computation of a cell's 100 nearest neighbors was performed in principle Component space after batch correction (50 Principal Components to be consistent with the downstream analysis of the integrated data). For the protocol-wise analysis, the integrated data was subset to *in vivo* and *in vitro* data of only the considered protocol. Since during Seurat CCA integration expression matrices are already subset to highly variable features, we only re-computed the Principal Component Analysis and subsequent nearest neighbor search ('FindNeighbors', based on Euclidean distance in the space spanned by the first 50 Principal Components) for the respective, batch-corrected subset. For a similar binary classification scheme as above, we computed a NEST-Score threshold based on the scenario that a cell's scaled neighborhood only originates from one of the two conditions. In more detail we compute the NEST-Score using

$$f_i^{scaled} = (1,0) \text{ and } f^{uniform} = (0.5,0.5)$$

resulting in value of  $-D_{KL}(f_i^{scaled} || f^{uniform}) = -1$ , which is also the minimal NEST-Score that can be attained in this setting. If a cell's NEST-Score was strictly larger than this threshold, i.e., if at least one cell from each condition was present in the neighborhood, the cell was labeled as *matched*. Otherwise, it was labeled as *in vivo/in vitro*-specific, depending on whether the cell is of *in vivo* or *in vitro* origin.

For pairwise comparisons of cell line y and cell line x, we compute the average of scaled contributions of x to a cell's neighborhood, i.e., the average of  $f_i^{scaled}(x)$ , across all cells i originating from cell line y. This is plotted as a heatmap, where y corresponds to a heatmap row and x to a heatmap column. Due to the normalization constant c, which is used for the computation of  $f_i^{scaled}(x)$ , the row sums of the corresponding heatmaps are 1.

### Module Score based on bulk RNA-seq differentially expressed marker genes

Per protocol, the top 50 differentially expressed genes (ranked by adjusted *p*-value) based on the bulk RNA-seq data across all considered experimental time points were input into Seurat's 'AddModuleScore' function<sup>57</sup> which calculates their average expression and rescales it with respect to a random control gene set.

### **Gene Ontology scores for scRNA-seq**

For one Gene Ontology term, genes attributed to this term were downloaded using the function 'select' of R package AnnotationDbi (v1.66.0) and package GO.db (v3.19.1) and input into Seurat's 'AddModuleScore' function.

### Integration of in vivo and in vitro scRNA-seq data

For fetal brain data published in Braun et al., <sup>24</sup> we merged already quality controlled samples that were sequenced in post-conceptional week 14 without any batch correction procedure as provided on https://github.com/linnarsson-lab/developing-human-brain (last access on July 16<sup>th</sup> 2024). Then, we followed a similar downstream analysis as for the *in vitro* data. We identified the most 3,000 highly variable genes, removed ribosomal and mitochondrial genes and MALAT1 from this list. Next, the *in vivo* and *in vitro* data were integrated using Seurat CCA: 1. Integration features ('SelectIntegrationFeatures', excluding mitochondrial and ribosomal genes and MALAT1) and subsequently integration anchors ('FindIntegrationAnchors', based on canonical correlation analysis 'CCA') were determined. After integrating the data with 'IntegrateData', downstream analysis was performed as described above to obtain the *in vitro* pan-protocol and pan-cell line UMAP embedding using the default of all 50 Principal Components. For visualization of clusters, we combined information of metadata 'Subregion' and 'CellClass' (Table S2). The alluvial plot in Figure 3F was plotted with R packages ggplot2 (v3.5.1) and ggalluvial (v0.12.5).

For fetal brain data published in Bhaduri et al., <sup>23</sup> we integrated high-quality cells from Gestational Weeks 14, 17 and 18 and excluded cells not listed in or labeled as 'Outlier' in the provided metadata. We randomly (stratified by cell type) subsampled 46,171 cells from the around 205,000 high-quality cells in Gestational Week 18, such that all considered *in vivo* cells in total add up to 70,000 cells roughly matching our *in vitro* dataset size. The *in vivo* was integrated with our *in vitro* data as described

### Resource



above, but due to visible batch effects between individuals, we split the considered *in vivo* data per individual ('14', '17', '18', '18\_2') and treated the respective 4 datasets as separate batches. Integration anchors ('FindIntegrationAnchors') were then computed by setting *in vitro* data as reference dataset. For visualization of clusters, we combined information of metadata 'structure' and 'cell\_type' (Table S2). For a straight-forward comparison with our *in vitro* dataset, brain region and cell type annotations of both *in vivo* datasets were aggregated hierarchically and renamed into simpler and coarser annotation names (Table S2).

### Time course bulk RNA-seq analysis

Reads were preprocessed using umi2index (Lexogen) to add the UMI sequence to the read identifier, and trimmed using BBDuk (v38.06) (ref = polyA.fa.gz,truseq.fa.gz k = 13 ktrim = r useshortkmers = t mink = 5 qtrim = r trimq = 10 minlength = 20). Reads mapping to abundant sequences included in the iGenomes UCSC hg38 reference (human rDNA, human mitochondrial chromosome, phiX174 genome, adapter) were removed using bowtie2<sup>52</sup> (v2.3.4.1) alignment. Remaining reads were analyzed using genome and gene annotation for the GRCh38/hg38 assembly obtained from Homo sapiens Ensembl release 94. Reads were aligned to the genome using star (v2.6.0c), alignments were processed using collapse\_UMI\_bam (Lexogen) and reads in genes were counted with featureCounts (subread v1.6.2) using strand-specific read counting (-s 1).

### **Pre-processing and downstream analysis**

For all bulk RNA-seq analysis, R (v4.4.0) was used. To address variable sequencing depths across samples we included only samples with more than 100,000 reads as high-quality samples in the analysis of the bulk RNA-seq data. For PCA read counts were normalized for library size to transcripts per million (TPM) and log2 transformed. Then the 2,000 most variable genes were selected and PCA was performed using the 'prcomp' command from the R package 'stats' (v4.4.0).

### **Explained variance by experimental condition**

To understand how much the individual factors influence gene expression, we first normalized the count data using the 'voom' function from limma<sup>35</sup> (v3.60.0). To ensure reliable analysis, genes with low expression were filtered out from the count matrix: Only genes that exhibited a counts-per-million (CPM) value of 5 or more in at least 20 samples were kept for subsequent normalization. With the R package variancePartition<sup>36</sup> (v1.34.0) and its function 'fitExtractVarPartModel' we then obtained estimates for how much variation of each gene was explained by the individual factors time, protocol and cell line. We multiplied the proportional explained variance of each gene for the different factors with the variance of the respective genes across the samples resulting in the fraction of explained variance per gene. Finally, to gauge the total impact of each factor on gene expression, we added up these individual contributions (fractional explained variance) per factor for all genes. For computing the explained variance of the factors over time we did the same as described above only for each time point individually.

### **Gene expression heatmaps and sample clustering**

For creating the heatmaps of the expression data counts were variance-stabilized using the 'vst' function from DESeq2<sup>56</sup> (v1.44.0), then mitochondrial and ribosomal genes were excluded from the variance-stabilized data and the plots created using the pheatmap package (v1.0.12) based on the 2,000 most variable genes.

### **Gene Ontology scores for bulk RNA-seq**

Bulk samples were stored as a merged Seurat Object and genes were retained if expressed in more than 10 samples. Default down-stream analysis was performed (treating one bulkRNA-seq sample as one 'cell'), i.e., log-normalization, determination of 2,000 highly variable genes and scaling. For one Gene Ontology term, genes attributed to this term were downloaded using the function 'select' of R package AnnotationDbi (v1.66.0) and package GO.db (v3.19.1) and input into Seurat's 'AddModuleScore' function.

### Protocol-specific marker genes

In order to find specific genes which are uniquely or predominantly expressed in each experimental protocol, we performed differential expression analysis on the voom normalized expression data. Using the R package limma (v3.60.0) we tested the expression of each gene in a given protocol across all cell lines against the average expression of the gene in all other protocols. We performed moderated t-tests, corrected the *p*-values via the Benjamini-Hochberg method and for each protocol considered the top 2,000 genes with adjusted *p*-value smaller 0.01. Genes were retained if the average log fold change was larger than 0.2. For a refined analysis of protocol-specific marker genes at day 40, we subset samples to day 40 and, for each protocol, tested cell lines yielding a minimum of 75% protocol-driven cells against remaining cell lines in this protocol and all cell lines in the other three protocols.